LICENTIATE THESIS

Clustering and caustics in one-dimensional models of turbulent aerosols

JAN MEIBOHM

Department of Physics
University of Gothenburg
Göteborg, Sweden 2018

Clustering and caustics in one-dimensional models of turbulent aerosols
Jan Meibohm

ISBN 978-91-7833-165-9 (PRINT)
ISBN 978-91-7833-166-6 (PDF)

This thesis is electronically published, available at
http://hdl.handle.net/2077/57538
https://github.com/jan-00-jan/Licentiate_thesis

Department of Physics
University of Gothenburg
SE-412 96 Göteborg
Sweden
Telephone: +46 (0)31-786 00 00

Front cover: A picture drawn by the author in the introductory course for Ph.D. students at Gothenburg University. Using this drawing, the author was supposed to explain to his fellow students what his research was going to be about.

Printed by BrandFactory AB
Göteborg, Sweden 2018

ABSTRACT

Heavy particles suspended in turbulent fluid flows, so-called turbulent aerosols, are common in Nature and in technological applications. A prominent example is rain droplets in turbulent clouds. Due to their inertia, ensembles of aerosol particles distribute inhomogeneously over space and can develop large relative velocities at small separations.

We use statistical models that mimic turbulent flow by means of Gaussian random velocity fields to describe these systems. Compared to models that involve actual turbulence, our statistical models are simpler to study and allow for an analytical treatment in certain limits. Despite their simplicity, statistical models qualitatively explain the results of direct numerical simulations and experiments.

In this Licentiate thesis, we focus primarily on studying one-dimensional versions of the statistical model. The results of these systems create intuition for, and give important insights into the behaviour of higher dimensional models of particles in turbulence.

List of papers

This thesis consists of an introductory text and the following three appended papers:

Paper A

Meibohm, J., Candelier, F., Rosen, T., Einarsson, J., Lundell, F. & Mehlig, B. 2016 Angular velocity of a spheroid log rolling in a simple shear at small Reynolds number. *Physical Review Fluids* **1** (8), 084203.

Paper B

Meibohm, J., Pistone, L., Gustavsson, K., & Mehlig, B. 2017 Relative velocities in bidisperse turbulent suspensions. *Physical Review E* **96** (6), 061102(R).

Paper C

Dubey, A., Meibohm, J., Gustavsson, K., & Mehlig, B. 2018 Fractal dimensions and trajectory crossings in correlated random walks. *arXiv e-print 1806.08207*

ACKNOWLEDGEMENTS

First and foremost, I would like to thank my supervisors Bernhard Mehlig and Kristian Gustavsson for taking me as a student and for creating a vibrant research environment.

Furthermore, I would like to thank our collaborators who I had the pleasure of working with: I thank Tomas Rosén, Fredrik Lundell and Lorenzo Pistone for interesting discussions and great numerical work. I am grateful to Fabien Candelier for introducing me to fluid dynamics and matched asymptotic expansions. Further, I would like to thank my office mates Johan and Anshuman for helping me with many different things and for making the office the fun place it is. Thanks also to Marina, Kristian, Erik and Anshuman for proofreading the thesis, and to Sophia for always being there.

CONTENTS

PART I
INTRODUCTION

Systems of heavy particles immersed in turbulent fluids, called turbulent aerosols, are abundant in Nature and technology [1, 2]. A prominent example is water droplets in warm stratocumulus clouds [3]. Cloud turbulence is believed to play an important role in the growth of droplets [4, 5]. When the droplets are small, they grow primarily through collisions, which are facilitated by the turbulence [6]. In order to understand the impact of turbulence on droplet growth, a detailed knowledge of the dynamics of turbulent aerosols is required. In particular, it is vital to understand how often the aerosol particles come close together and, when they do, how fast they move relative to each other [7, 8, 9, 10]. Due to particle inertia, heavy particles may cross the stream lines of the underlying fluid and engage in spatial clustering [1, 2, 11, 12, 13, 14]. Clustering describes the phenomenon that ensembles of heavy particles, instead of distributing homogeneously over space, form regions of high (and low) concentration even though the underlying turbulent fluid may be incompressible. At the same time, particles with different acceleration histories may approach each other at high relative velocities due to caustic singularities in the inertial particle dynamics [6, 7, 8, 9, 10, 15], which affects the rate and outcomes of collisions [2].

Models based on a probabilistic approach to turbulence, called statistical models in the literature [1], have helped considerably in the understanding of the dynamics of turbulent aerosols. These models abandon the ambitious endeavour of describing the underlying turbulence and instead model the fluid by a random velocity field [11, 16]. The particle dynamics is subject to forces induced by the random fluid field fluctuations. Using statistical models, we can study the mechanisms of spatial clustering and the relative velocity statistics in a simplified environment. Yet these models are realistic enough to qualitatively explain the results of turbulence simulations and experiments [1].

In this Licentiate thesis, we review known results and discuss recent progress in the study of statistical models for turbulent aerosols. We focus

primarily on one-dimensional versions of the model, for which analytical results can be obtained. Known models of this type are the white-noise model [1] and the telegraph model [17]. We introduce a new system with this property, the persistent-flow model, which is valid for weakly inertial particles in a highly persistent flow. Despite the apparent simplicity of these one-dimensional models, they are surprisingly rich in their dynamics and provide valuable insights for higher dimensional systems [1, 6, 18]. This aspect is shown and discussed in the research papers appended to the text.

The thesis is organised as follows: After moving step-by-step from the complex problem of inertial particles in turbulence to statistical models in Chapter 1, we discuss the phenomenon of spatial clustering in Chapter 2. In Chapters 3 we review and extend the knowledge of spatial clustering in one-dimensional statistical models. The research papers produced in the course of three year's work are reviewed and put into the context of the preceding text in Chapter 4. Conclusions are drawn and possible future projects are discussed in Chapter 5.

This Licentiate thesis is intended to give the interested reader an intelligible and concise introduction to the world of one-dimensional statistical models of turbulent aerosols. In the author's personal view, the papers B and C showcase the value of these models. Paper A discusses the angular velocity of a *single* particle in a shear flow and is slightly detached from the rest of the work.

1 Particles in fluids

The motion of an ensemble of non-interacting spherical particles in fluid turbulence is a complex problem to study [1, 2, 6]. This becomes clear already when considering the motion of a single particle. On the one hand, the fluid motion, possibly a very complicated motion in itself, applies a force on the particle which makes it move. The moving particle, on the other hand, pushes aside the fluid, generating a complicated disturbance of the flow. Such disturbances may, depending on the viscosity of the fluid, persist for some time and affect the particle motion later. If more particles are involved, other effects such as hydrodynamic interactions between the particles come into play [19, 20]. Due to the complexity of the system, the main challenge is to find a way of simplifying the problem without losing the essential physics. Before discussing the approximations and simplifications we are going to make in this work, we describe the system on a more formal level.

1.1 Problem formulation

The dynamics of particles in an incompressible fluid is described by the Navier-Stokes equations [21, 22, 23]

$$\frac{\partial \boldsymbol{w}}{\partial t} + (\boldsymbol{w}\cdot\nabla)\boldsymbol{w} = -\nabla p - \nu\nabla^2\boldsymbol{w}\,, \tag{1.1a}$$

$$\nabla\cdot\boldsymbol{w} = 0\,. \tag{1.1b}$$

Here, $\boldsymbol{w}(\boldsymbol{x},t)$ and $p(\boldsymbol{x},t)$ are the velocity of the fluid and the pressure at position $\boldsymbol{x}$ and time t, respectively. The quantity ν denotes the kinematic viscosity of the fluid. The first equation (1.1a) can be identified as Newton's second law for an infinitesimal fluid parcel. Eq. (1.1b) ensures incompressibility of the flow. First, we note that the Navier-Stokes equations are non-linear, because of the so-called convective term $(\boldsymbol{w}\cdot\nabla)\boldsymbol{w}$ on the left hand side of Eq. (1.1a). This non-linearity has drastic and important consequences that we describe later in this Section. The term $-\nu\nabla^2\boldsymbol{w}$ on the right-hand side of the equation is called the viscous term. It is responsible for the dissipation of energy in the fluid. Because of the viscous term, perturbations of the flow smoothen out with time. For our purposes, the Navier-Stokes equations need to be supplemented by suitable boundary conditions that account for the

presence of the particles. The no-slip boundary condition is used in viscous flows. It requires that the fluid velocity relative to the surface of the particles must vanish [19, 20]. The no-slip boundary condition leads to fluid stresses on the particle surfaces which in turn result in forces that make the particles move [19, 20].

There are two fundamental difficulties in describing the above system. The first one arises, because the problem requires the simultaneous solution of the field equations (1.1), while satisfying the boundary conditions which change as a function of time as the particles move through the fluid. Problems like this require so-called self-consistent solutions that are challenging to obtain even for a small number of particles [19, 20]. Second, if the fluid moves quickly, the non-linear term in Eq. (1.1a) renders the solutions of the Navier-Stokes equations unstable, leading to chaotic fluid motion. In fluid dynamics, this is known as turbulence [22, 23]. These difficulties make the complete problem intractable and call for approximations. We explain these approximations in the Sections that follow.

1.2 One-way coupling approximation

First, we assume that the particle system is so dilute that there are no hydrodynamic interactions between the particles. This is typically the case in, for instance, turbulent air clouds [1]. Note, however, that when there is strong spatial clustering of the particles, this assumption may break down [1, 24]. Second, we assume that the particles are much smaller than the smallest structures of the flow. Because of the viscous term, such a smallest spatial scale exists, a fact we discuss in the next Section.

These assumptions motivate the 'one-way coupling' approximation [25]. It assumes that the presence of the particles changes the flow only marginally so that the boundary condition can be disregarded in Eqs. (1.1). That is to say, the motion of the particles is influenced by the fluid flow, but the flow-field, on the other hand, is not affected by the particles. The one-way coupling approximation is useful because it decouples the flow-field motion from the motion of the particles, making the problem more tractable. Once the equations are decoupled, we can discuss turbulence and the particle motion separately.

1.3 Turbulence

Turbulence is the most common state of fluids in Nature. It describes the chaotic and strongly mixing behaviour of rapidly moving fluids and is caused by the non-linearity of the problem (1.1) [22]. Despite its long history, turbulence is still an active field of research and the non-linear field equations (1.1) remain a major challenge. Since the times of Navier and Stokes the understanding of turbulence has improved considerably [26], while several fundamental problems remain unsolved. In this Section, we describe important aspects of turbulence on a phenomenological level. A better understanding of the existence of a smallest scale in turbulence and the origin of the highly irregular motion in turbulent flows motivates the main ingredient to our model for turbulent aerosols, the random flow field. For a detailed account of turbulence see Refs. [22] and [23].

1.3.1 Reynolds number

Given a length scale L and a velocity scale V, we can construct the dimensionless Reynolds number

$$\mathrm{Re} = \frac{LV}{\nu}\,, \tag{1.2}$$

which characterises the flow behaviour [19, 22]. In simple systems such as the flow of water through a pipe, there is a *single* Reynolds number that characterises the motion of the fluid, regardless of the magnitudes of the individual quantities in Eq. (1.2). The significance of Re becomes clear when transforming the variables in the Navier-Stokes equations (1.1a) according to $\boldsymbol{w} \to V\boldsymbol{w}$, $\boldsymbol{x} \to L\boldsymbol{x}$, $t \to (L/V)t$ and $p \to (V\nu/L^2)p$. One obtains the dimensionless equation

$$\mathrm{Re}(\partial_t \boldsymbol{w} + (\boldsymbol{w}\cdot\nabla)\boldsymbol{w}) = -\nabla p - \nabla^2 \boldsymbol{w}\,, \tag{1.3}$$

that depends only on the Reynolds number, and possibly on the boundary conditions. Because Re appears on the left-hand side of Eq. (1.3), it controls the importance of the terms $\partial_t \boldsymbol{w}$ and $(\boldsymbol{w}\cdot\nabla)\boldsymbol{w}$. As mentioned earlier, the non-linear convective term $(\boldsymbol{w}\cdot\nabla)\boldsymbol{w}$ is responsible for the onset of turbulence. At small Re, the non-linearity is negligible and Eq. (1.3) can be treated as effectively linear. Solutions of the linearised equations are stable and possibly

steady. In particular, these flows do not mix and individual fluid parcels move along stream lines. Flows with these properties are called laminar [19].

If we want to describe more complex systems than a simple pipe flow, the construction of the Reynolds number according to Eq. (1.2) is no longer unique. Consequently, fluid dynamical problems that contain several length and/or velocity scales, are characterised by several different Reynolds numbers. Thus for a finite-size particle moving in a pipe flow, we have a flow Reynolds number associated to the motion of the fluid in the pipe and a particle Reynolds number associated to the relative motion of the particle and the fluid.

We now discuss a fluid at large Reynolds number, $\mathrm{Re} \gg 1$. In this case, the non-linear term renders the flow unstable and we expect the fluid motion to be highly irregular and complicated. Observations of fluid flows at high Reynolds numbers indicate, however, that statistical averages of turbulent flows are highly symmetric. Loosely speaking, the flow looks irregular and complicated in the same way everywhere and for all times. This simple argument describes the important concept of statistical homogeneity and isotropy of turbulent flow [22, 23]. If the Reynolds number is large enough, suitably defined statistical observables of the flow, such as correlation functions, are invariant under translations and rotations.

1.3.2 Turbulent cascade

It is instructive to think that turbulent fluid motion is characterised by eddies of different sizes. Think of a cup of coffee and add a little milk to it. Not much happens so far, but as soon as we start to stir the mixture with a spoon, eddies of approximately the size of the spoon form. These eddies are unstable and break up into smaller eddies, which again decompose into even smaller ones [22]. In the coffee cup we now suddenly see a lot of structure. A whole ensemble of eddies of different sizes interact with each other, engaging in the formation of complex patterns. If we were to zoom in into these patterns very closely, we would realise that there is a finite end to the structure in the fluid. At small scales, depending how thick, or viscous, the coffee and the milk are, the eddy-structure so predominant at larger scales, is gone. The internal friction of the fluid efficiently smoothens out all small structures below a certain length scale, called the Kolmogorov length η_{K} [22, 23, 27, 28].

In the turbulence literature, the ensemble of eddies of different sizes is

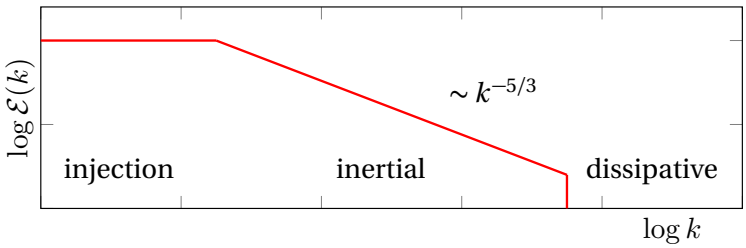

Figure 1.1: Schematic of the energy spectrum $\mathcal{E}(k)$ as a function of k.

called the 'Richardson' or 'energy' cascade [22, 29], because it transports the injected energy at large length scales (stirring with the spoon) to ever smaller scales until it is eventually dissipated into heat at scales of the order of η_K.

Eddies of size l have an associated wave number $k \sim 1/l$. Hence, small spatial scales correspond to large k-values whilst large spatial scales correspond to small k. We define the scale-dependent quantity $\mathcal{E}(k)$ to be the energy content of eddies with wave number k [23]. In a famous series of papers, Kolmogorov [27, 28] used symmetry and universality arguments to describe $\mathcal{E}(k)$ for isotropic and homogeneous turbulence. His result is shown schematically as the red line in Fig. 1.1. The flat regime at small k is the scale associated to energy injection, called the 'injection scale'. The energy that is brought into the system at these large length scales (small k) is transported to smaller scales (larger k) by means of the Richardson cascade described above. Kolmogorov was able to show that on the basis of his assumptions, $\mathcal{E}(k)$ has a power-law form with exponent approximately $-5/3$ at wave numbers sufficiently larger than the injection scale [27, 28]. This regime is called the 'inertial range'. At large k and small length scales of the order of η_K, this power law is cut off by dissipation and, hence, by the viscosity of the fluid, in a regime called the 'dissipative range'.

As noted in Section 1.2 we want to describe systems in which the particles are smaller than the Kolmogorov length. It has been shown that the length scales where the fluid-velocity field is smooth can extend up to several η_K, depending on the Reynolds number [1, 30]. We may therefore assume that the fluid flow which the particles experience is smooth.

1.3.3 Gaussian random-flow model

We now condense the insights gained in the previous Section into a simple fluid model. Because the detailed turbulent motion at high Reynolds numbers is highly irregular, it is practically unpredictable. For systems like this, it makes sense to consider its long-time statistical properties instead of trying to predict individual realisations [22, 23, 31]. Here, we go one step further and adopt a drastic simplification that lies at the heart of the statistical description of turbulence. We construct models that put emphasis only on modelling the *statistics* of the flow field $\boldsymbol{w}(\boldsymbol{x},t)$, not its individual realisations [1]. At first sight, this may not appear to be a great simplification. However, it allows us to abandon the idea of solving the Navier-Stokes equations (1.1) and, thus turbulence, all together. Instead, we introduce a field $\boldsymbol{u}(\boldsymbol{x},t)$ with statistical properties that are similar to those of $\boldsymbol{w}(\boldsymbol{x},t)$ in the dissipative range. To this end, we define a d-dimensional random field $\boldsymbol{\phi}(\boldsymbol{x},t)$ in a periodic box of size L by [1, 11]

$$\boldsymbol{\phi}(\boldsymbol{x},t) = N_d \sum_{\boldsymbol{k}} \boldsymbol{a}_{\boldsymbol{k}}(t) f(\boldsymbol{k}) \mathrm{e}^{i\boldsymbol{k}\cdot\boldsymbol{x}}, \tag{1.4}$$

where $\boldsymbol{k} \in (2\pi/L)\mathbb{Z}^d$ and N_d is a normalisation constant that depends on d. Furthermore, for a given $\boldsymbol{k}$, $\boldsymbol{a}_{\boldsymbol{k}}(t)$ is a stationary, complex d-dimensional random process and f is a function of $\boldsymbol{k}$ that we specify below. Since $\boldsymbol{\phi}$ is real, we need to add the condition that $\boldsymbol{a}^*_{\boldsymbol{k}}(t) = \boldsymbol{a}_{-\boldsymbol{k}}(t)$.

In this work, we use two and three dimensional incompressible random velocity fields defined by

$$\boldsymbol{u}(\boldsymbol{x},t) = \boldsymbol{\nabla} \wedge \boldsymbol{\phi}(\boldsymbol{x},t). \tag{1.5}$$

One-dimensional fields, however, can always be expressed in terms of the derivative of a potential and are hence compressible. Therefore, we define one-dimensional *compressible* velocity fields as

$$u(x,t) = \partial_x \phi(x,t). \tag{1.6}$$

Note that we have defined the random field (1.4) so that spatial and time correlation factorise if the processes $a_{i,\boldsymbol{k}}(t)$ are independent. To see this consider the correlation function

$$\langle \phi_i(\boldsymbol{x},t)\phi_j(\boldsymbol{y},s)\rangle = N_d^2 \sum_{\boldsymbol{k},\boldsymbol{l}} \langle a_{i,\boldsymbol{k}}(t) a_{j,\boldsymbol{l}}(s)\rangle f(\boldsymbol{k}) f(\boldsymbol{l}) \mathrm{e}^{i(\boldsymbol{k}\cdot\boldsymbol{x}+\boldsymbol{l}\cdot\boldsymbol{y})}. \tag{1.7}$$

Clearly, if $a_{i,\boldsymbol{k}}$ are independent so that $\langle a_{i,\boldsymbol{k}}(t)a^*_{j,\boldsymbol{l}}(s)\rangle = C(|t-s|)\delta_{ij}\delta_{\boldsymbol{kl}}$, Eq. (1.7) factorises and we find

$$\langle \phi_i(\boldsymbol{x},t)\phi_j(\boldsymbol{y},s)\rangle = \delta_{ij}C(|t-s|)G(\boldsymbol{x}-\boldsymbol{y}), \tag{1.8}$$

where $G(\boldsymbol{x}) = N_d^2 \sum_{\boldsymbol{k}} f(\boldsymbol{k})^2 \mathrm{e}^{i\boldsymbol{k}\cdot\boldsymbol{x}}$ is proportional to the Fourier transform of $f(\boldsymbol{k})^2$. Note further that using this construction, the statistics of $\boldsymbol{\phi}(\boldsymbol{x},t)$ at each point $\boldsymbol{x}$ in space is determined by the statistics of the underlying random process $\boldsymbol{a}_{\boldsymbol{k}}(t)$, while its time correlation is fixed by the time correlation of $\boldsymbol{a}_{\boldsymbol{k}}(t)$. The spatial correlation $G(\boldsymbol{x})$, on the other hand, depends only on the choice of the function $f(\boldsymbol{k})$. These conclusions apply in a similar way to the higher moments of $\boldsymbol{\phi}(\boldsymbol{x},t)$.

The above construction allows to generate random fields with a large variety of different statistics. Generalisations of the procedure using $\boldsymbol{k}$-dependent processes $\boldsymbol{a}_{\boldsymbol{k}}(t)$ are straightforward in principle. In the rest of this work, we choose $\boldsymbol{a}_{\boldsymbol{k}}(t)$ to be independent Ornstein-Uhlenbeck processes. Their components have Gaussian statistics and individual realisations are solutions of the stochastic differential equations

$$\dot{a}_{i,\boldsymbol{k}}(t) = -\frac{a_{i,\boldsymbol{k}}(t)}{\tau} + \sqrt{2D}\,\xi_{i,\boldsymbol{k}}(t), \tag{1.9}$$

where $\xi_{i,\boldsymbol{k}}(t)$ are complex Gaussian white noises with correlation

$$\langle \xi_{i,\boldsymbol{k}}(t)\xi^*_{j,\boldsymbol{l}}(s)\rangle = \delta_{ij}\delta_{\boldsymbol{kl}}\delta(t-s). \tag{1.10}$$

Choosing Ornstein-Uhlenbeck processes for $\boldsymbol{a}_{\boldsymbol{k}}(t)$ renders $\boldsymbol{\phi}(\boldsymbol{x},t)$ Gaussian with time correlation

$$C(|t-s|) = 2\tau^{-1}\mathrm{e}^{-|t-s|/\tau}, \tag{1.11}$$

which implies that τ is the correlation time of $\boldsymbol{\phi}(\boldsymbol{x},t)$. A convenient choice for $f(\boldsymbol{k})$ is $f(\boldsymbol{k}) = \mathrm{e}^{-\eta^2 k^2/4}$, for which we obtain the spatial correlation

$$G(\boldsymbol{x}) \sim \eta^{-d}\mathrm{e}^{-x^2/(2\eta^2)} \tag{1.12}$$

in the limit $L \to \infty$.

Using Gaussian statistics has the advantage of being computationally convenient. However, turbulence fluid velocities can be shown to be highly

non-Gaussian in the dissipative range, due to 'intermittency' [23] which describes sudden strong outbursts of turbulent fluctuations. Furthermore, real turbulence exhibits long-lived regions of high vorticity, so-called vortex tubes [32] that are absent in the statistical model. Finally, the dissipation in Eq. (1.1) and, hence, the Richardson cascade break time-reversal symmetry in turbulence [23], while the statistical model is time-reversal symmetric [1]. These shortcomings of the statistical model have measurable consequences when compared *quantitatively* to direct numerical simulations [1]. The simplicity of the model and its ability of *qualitatively* explaining more complicated systems makes it, however, attractive for further studies.

A more detailed account on the construction of the random flow, including also higher-order correlations $\boldsymbol{\phi}$ is found in Refs. [1, 33].

1.4 Particle motion in a fluid

As the second part of our problem, we need to understand how particles move in a generic flow. That is, we require the forces that act on the particles for a given flow field. Depending on how large the impact of the presence of the particle on the flow field is, the non-linear term $(\boldsymbol{w}\cdot\nabla)\boldsymbol{w}$ can become relevant. Reliable analytical expressions for the force on the particle can be formulated only for laminar flows when the particle moves slowly relative to the fluid [19, 20, 34]. For these flows, the Reynolds number associated to the particle motion, is small.

1.4.1 Low-Reynolds-number flows

In order to know when the force on a particle generated by a laminar flow is a good approximation in turbulence, we need to compare the size of the non-linear term in Eq. (1.1a) to that of the other terms. This is done by considering the particle Reynolds number Re_p, which is obtained from using Eq. (1.2) with the size a of the particle as the length scale and its velocity v_0 relative to the flow as the velocity scale. We obtain

$$\mathrm{Re}_\mathrm{p} = v_0 a/\nu. \tag{1.13}$$

Naively, when $\mathrm{Re}_\mathrm{p} \ll 1$ the left hand of Eq. (1.3) is negligible and we can consider the so-called Stokes equation [19, 20]

$$\nabla p + \nabla^2 \boldsymbol{w} = 0. \tag{1.14}$$

A more detailed analysis, however, reveals that the left-hand side of Eq. (1.3) is a singular perturbation to Eq. (1.14) [35]. One way of solving such boundary-layer problems is by using matched asymptotic expansions [36, 37]. Applying this method one solves two or sometimes even more different perturbation problems inside and outside the boundary layer(s) and matches them together. This method allows to obtain the force on a spherical particle given the unperturbed ambient flow without the particle [35]. For a very small particle, that moves slowly relative to the flow and is much denser than fluid, it is a good approximation to use a constant ambient flow to calculate the force [1]. The corresponding equation for the force is known as Stokes law [19, 20]

$$\boldsymbol{F} = 6\pi\nu\rho_{\mathrm{f}} a(\boldsymbol{w}(\boldsymbol{x},t)-\boldsymbol{v}(t)), \tag{1.15}$$

where ρ_{f} denotes the fluid density. Note that we have neglected gravity [38, 39, 40, 41] because we solely focus on inertial effects here. The linearity of Eq. (1.15) in $\boldsymbol{w}(\boldsymbol{x},t)$ makes the problem tractable both numerically and, in some cases, even analytically.

1.5 The statistical model

We are now in the position to formulate the system of equations that makes up the statistical model for turbulent aerosols [1]. Using Stokes law (1.15) with the fluid velocity field $\boldsymbol{w}(\boldsymbol{x},t)$ replaced by the random velocity field $\boldsymbol{u}(\boldsymbol{x},t)$, we obtain the equations of motion for a single particle

$$\tfrac{\mathrm{d}}{\mathrm{d}t}\boldsymbol{x}(t) = \boldsymbol{v}(t), \tag{1.16a}$$

$$\tfrac{\mathrm{d}}{\mathrm{d}t}\boldsymbol{v}(t) = \gamma(\boldsymbol{u}(\boldsymbol{x}(t),t)-\boldsymbol{v}(t)), \tag{1.16b}$$

where $\gamma = 9/2(\rho_{\mathrm{f}}/\rho_{\mathrm{p}})(\nu/a^2)$ is called the viscous damping and ρ_{p} is the density of the particle. The random velocity field $\boldsymbol{u}(\boldsymbol{x},t)$ has the first and second moments (see Section 1.3.3)

$$\langle \boldsymbol{u}(\boldsymbol{x},t)\rangle = 0 \tag{1.17a}$$

$$\langle u_i(\boldsymbol{x},t)u_j(\boldsymbol{y},t)\rangle = u_0^2\left[1-\frac{(\boldsymbol{x}-\boldsymbol{y})^2}{\eta^2}\right]\delta_{ij}\mathrm{e}^{-(\boldsymbol{x}-\boldsymbol{y})^2/(2\eta^2)}\mathrm{e}^{-|t-s|/\tau}. \tag{1.17b}$$

Because $\boldsymbol{u}(\boldsymbol{x},t)$ is taken to be Gaussian, its statistics is completely described by Eqs. (1.17). Recall from Section 1.2 that we treat the interaction of the

particle with the fluid within the one-way coupling approximation, so that adding additional non-interacting particles to the fluid does not alter the equations. In particular, we can define a whole ensemble of particles and treat them as the field $\boldsymbol{x}(t) = \boldsymbol{x}(\boldsymbol{x}_0, t)$ which maps an initial particle position $\boldsymbol{x}_0$ at some initial time t_0 to a final position $\boldsymbol{x}(t)$ at time t. This particle field has an associated velocity field that we call $\boldsymbol{v}(\boldsymbol{x}(t), t) = \partial_t \boldsymbol{x}(\boldsymbol{x}_0, t)$. These two fields satisfy the same equations of motion as the single particle in Eq. (1.16). We have

$$\frac{\mathrm{d}}{\mathrm{d}t}\boldsymbol{x}(\boldsymbol{x}_0, t) = \boldsymbol{v}(\boldsymbol{x}(t), t), \tag{1.18a}$$

$$\frac{\mathrm{d}}{\mathrm{d}t}\boldsymbol{v}(\boldsymbol{x}(t), t) = \gamma(\boldsymbol{u}(\boldsymbol{x}(t), t) - \boldsymbol{v}(\boldsymbol{x}(t), t)). \tag{1.18b}$$

From now on, we use the short-hand notation $\boldsymbol{x}(t) = \boldsymbol{x}(\boldsymbol{x}_0, t)$ and $\boldsymbol{v}(t) = \boldsymbol{v}(\boldsymbol{x}(t), t)$. It is worth mentioning that the fields $\boldsymbol{x}(t)$ and $\boldsymbol{v}(t)$ are in general multivalued [6, 7, 8], due to caustics in the particle dynamics described later. For most purposes in this work, it is convenient to also consider the equations of motion for the tensor quantities [1, 6, 42]

$$\mathbb{J}(t) = \mathbb{J}(\boldsymbol{x}(t), t) = \frac{\partial \boldsymbol{x}(\boldsymbol{x}_0, t)}{\partial \boldsymbol{x}_0}, \tag{1.19a}$$

$$\mathbb{Z}(t) = \mathbb{Z}(\boldsymbol{x}(t), t) = \frac{\partial \boldsymbol{v}(\boldsymbol{x}(t), t)}{\partial \boldsymbol{x}(t)}, \tag{1.19b}$$

in addition to Eqs. (1.16). Taking partial derivatives of Eqs. (1.18) with respect to $\boldsymbol{x}_0$ and $\boldsymbol{x}(t)$, respectively, and using the definitions (1.19), we obtain

$$\frac{\mathrm{d}}{\mathrm{d}t}\mathbb{J}(t) = \mathbb{Z}(t)\mathbb{J}(t), \tag{1.20a}$$

$$\frac{\mathrm{d}}{\mathrm{d}t}\mathbb{Z}(t) = \gamma[\mathbb{A}(t) - \mathbb{Z}(t)] - \mathbb{Z}(t)^2, \tag{1.20b}$$

where $\mathbb{A}(t) = \partial \boldsymbol{u}(\boldsymbol{x}(t), t)/\partial \boldsymbol{x}(t)$ is the field of fluid velocity gradients. Furthermore, $\mathbb{J}(t)$ has the initial condition $\mathbb{J}(t_0) = \mathbb{1}$.

1.5.1 Dimensionless variables

In our approximation, the whole particle-fluid system depends only on the four parameters γ, u_0, η and τ. Dedimensionalising Eqs. (1.18) with these parameters, one finds that the system is in fact characterised by only two dimensionless numbers which we call the Stokes and the Kubo numbers

[1]. The Stokes number $\mathrm{St} = 1/(\gamma\tau)$ measures the relevance of particle inertia while the Kubo number $\mathrm{Ku} = u_0\tau/\eta$ is a measure for the persistence of the flow. In this short Section, we give an overview over the two dedimensionalisation schemes – we call them the Stokes and the Kubo coordinates – that we will use in the rest of the work. We first perform the coordinate transform $t \to t/\gamma$, $\boldsymbol{u} \to \eta\gamma\boldsymbol{u}$, $\boldsymbol{x} \to \eta\boldsymbol{x}$ and $\boldsymbol{v} \to \eta\gamma\boldsymbol{v}$ and obtain the dimensionless equations [1]

$$\frac{\mathrm{d}}{\mathrm{d}t}\boldsymbol{x}(t) = \boldsymbol{v}(t), \tag{1.21a}$$

$$\frac{\mathrm{d}}{\mathrm{d}t}\boldsymbol{v}(t) = \boldsymbol{u}(\boldsymbol{x}(t),t) - \boldsymbol{v}(t), \tag{1.21b}$$

$$\frac{\mathrm{d}}{\mathrm{d}t}\mathbb{J}(t) = \mathbb{Z}(t)\mathbb{J}(t), \tag{1.21c}$$

$$\frac{\mathrm{d}}{\mathrm{d}t}\mathbb{Z}(t) = \mathbb{A}(t) - \mathbb{Z}(t) - \mathbb{Z}(t)^2, \tag{1.21d}$$

$$\langle u_i(\boldsymbol{x},t)u_j(\boldsymbol{y},t)\rangle = \mathrm{Ku}^2\mathrm{St}^2\left[1-(\boldsymbol{x}-\boldsymbol{y})^2\right]\delta_{ij}\mathrm{e}^{-(\boldsymbol{x}-\boldsymbol{y})^2/2}\mathrm{e}^{-\mathrm{St}|t-s|}, \tag{1.21e}$$

For lack of a better name, we call this first dedimensionalisation the Stokes coordinates. This scheme is useful because it makes the particle equations of motion independent of Ku and St. A second rescaling of Eqs. (1.16) reads $t \to \tau t$, $\boldsymbol{u} \to u_0\boldsymbol{u}$, $\boldsymbol{x} \to \eta x$ and $\boldsymbol{v} \to u_0\boldsymbol{v}$, and leads to a parameter-independent correlation function. We have [1]

$$\frac{\mathrm{d}}{\mathrm{d}t}\boldsymbol{x}(t) = \mathrm{Ku}\,\boldsymbol{v}(t), \tag{1.22a}$$

$$\frac{\mathrm{d}}{\mathrm{d}t}\boldsymbol{v}(t) = \mathrm{St}^{-1}\left[\boldsymbol{u}(\boldsymbol{x}(t),t) - \boldsymbol{v}(t)\right], \tag{1.22b}$$

$$\frac{\mathrm{d}}{\mathrm{d}t}\mathbb{J}(t) = \mathrm{Ku}\,\mathbb{Z}(t)\mathbb{J}(t) \tag{1.22c}$$

$$\frac{\mathrm{d}}{\mathrm{d}t}\mathbb{Z}(t) = \mathrm{St}^{-1}\left[\mathbb{A}(t) - \mathbb{Z}(t)\right] - \mathrm{Ku}\,\mathbb{Z}(t)^2, \tag{1.22d}$$

$$\langle u_i(\boldsymbol{x},t)u_j(\boldsymbol{y},t)\rangle = \left[1-(\boldsymbol{x}-\boldsymbol{y})^2\right]\delta_{ij}\mathrm{e}^{-(\boldsymbol{x}-\boldsymbol{y})^2/2}\mathrm{e}^{-|t-s|}. \tag{1.22e}$$

We call the coordinates that correspond to Eqs. (1.22) Kubo coordinates, because they are used in an approximation scheme called the Kubo expansion [1, 43]. Both sets of dimensionless variables are used in this work, because each of them is convenient for different purposes.

We have come a long way from considering the very complicated problem of inertial particles in turbulence to the equations of motion for a field of particles in a random velocity field. The next Sections will teach us how rich the dynamics of Eqs. (1.20)-(1.22) is, even after the drastic simplifications we have made. Furthermore, comparisons with the results of direct numerical simulations summarised in Ref. [1] suggest that the statistical model

is capable of explaining these results *qualitatively* and in some cases even *quantitatively*.

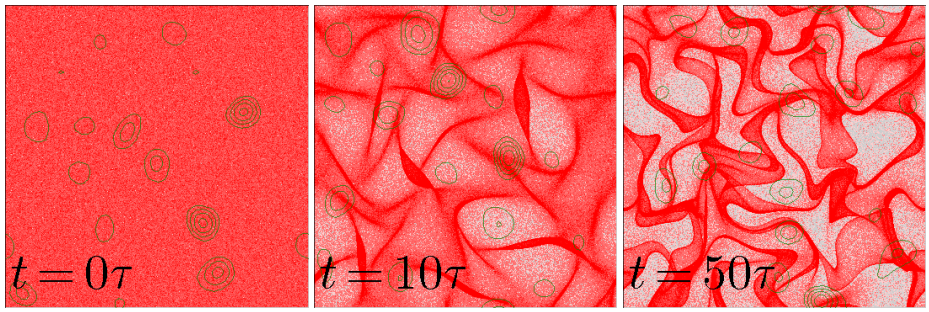

Figure 2.1: An initially homogeneous distribution of inertial particles (red) clusters in a random flow. The green lines are level lines of fluid vorticity. The Kubo and Stokes numbers are 0.1 and 10, respectively. The Figures were generated by Kristian Gustavsson and are used with permission.

2 Spatial clustering

Spatial clustering describes the formation of regions of high concentration of aerosol particles [11, 13, 14, 44, 45, 46]. Neutrally buoyant, infinitesimally small particles, called tracers, distribute homogeneously over space if the underlying turbulent flow is incompressible [26]. This is because the particle motion is restricted to the stream lines of the flow. For aerosol particles which are heavier than the fluid, this is no longer true. In this case, the particles may detach from the flow. This implies that the particle dynamics takes place in the higher-dimensional phase space and gives rise to a whole spectrum of different competing mechanisms that eventually contribute to particle clustering. Fig. 2.1 shows how an initially homogeneously distributed set of heavy (red) particles at $t = 0$ (left panel) forms regions of high and low concentration over the course of 50 fluid correlation times τ. Clustering increases the probability of particles to come close together, thereby drastically increasing collision rates [2, 13]. This is important in turbulent air clouds, where the formation of regions of high water droplet concentration is believed to increase the probability of droplet collisions, and hence facilitate droplet growth [2, 4, 26].

In this Chapter we first discuss the physical mechanisms behind particle clustering. After that we introduce observables that characterise the phenomenon and explain in which way they are relevant.

2.1 Origins of clustering

There are three main mechanisms that are known to be important for spatial particle clustering in incompressible flows. These are preferential concentration, phase-space contraction and multiplicative amplification, and caustics [1]. We explain these mechanisms in the following and briefly mention the effect of flow compressibility which is relevant in the one-dimensional models.

2.1.1 Preferential concentration

As discussed in Section 1.3, turbulence can be seen as an ensemble of vortices of different sizes. Loosely speaking, these vortices force tracer particles to roughly follow circular orbits. Heavy particles, on the other hand, spiral out of vortices because of centripetal forces, and they accumulate in regions of low vorticity and high strain. This was first noted by Maxey [39] who used an expansion around the limit $\mathrm{St}=0$, to argue for this. His approach is sketched in what follows. We start with the equations of motion in Kubo coordinates

$$\frac{\mathrm{d}}{\mathrm{d}t}\boldsymbol{x}(t)=\mathrm{Ku}\,\boldsymbol{v}(t), \tag{2.1a}$$

$$\frac{\mathrm{d}}{\mathrm{d}t}\boldsymbol{v}(t)=\mathrm{St}^{-1}\left[\boldsymbol{u}(\boldsymbol{x}(t),t)-\boldsymbol{v}(t)\right], \tag{2.1b}$$

$$\frac{\mathrm{d}}{\mathrm{d}t}\mathbb{J}(t)=\mathrm{Ku}\,\mathbb{Z}(t)\mathbb{J}(t) \tag{2.1c}$$

$$\frac{\mathrm{d}}{\mathrm{d}t}\mathbb{Z}(t)=\mathrm{St}^{-1}\left[\mathbb{A}(t)-\mathbb{Z}(t)\right]-\mathrm{Ku}\,\mathbb{Z}(t)^2, \tag{2.1d}$$

and treat the Stokes number as small. We take the underlying flow field to be incompressible and assume that all quantities can be expanded in a power series in St, the smallest order being the dynamics of tracer particles. Substituting these series expansions into Eq. (2.1), we can evaluate order by order in St and obtain a hierarchy of equations, one for each order in St. A perturbative solution for $\mathbb{Z}(t)$ can now be straightforwardly obtained. One finds to order $\mathcal{O}(\mathrm{St})$ [1, 39]

$$\mathbb{Z}(t)\sim\mathbb{A}^{(0)}(t)+\mathrm{St}\left\{\mathbb{A}^{(1)}(t)-\tfrac{\mathrm{d}}{\mathrm{d}t}\mathbb{A}^{(0)}(t)-\mathrm{Ku}\left[\mathbb{A}^{(0)}(t)\right]^2\right\}, \tag{2.2}$$

where $\mathbb{A}^{(i)}(t)=\partial^i_{\mathrm{St}}\mathbb{A}(\boldsymbol{x}(t),t)|_{\mathrm{St}=0}$. Taking the trace of Eq. (2.2) and using $\mathrm{Tr}\,\mathbb{Z}=\nabla\cdot\boldsymbol{v}$, Maxey found that [39]

$$\nabla\cdot\boldsymbol{v}\sim-\mathrm{Ku}\,\mathrm{St}\,\mathrm{Tr}\left[\mathbb{A}^{(0)}(t)\right]^2=\mathrm{Ku}\,\mathrm{St}(\mathrm{Tr}\,\mathbb{O}^{(0)}\mathbb{O}^{(0)T}-\mathrm{Tr}\,\mathbb{S}^{(0)}\mathbb{S}^{(0)T}). \tag{2.3}$$

Here, $\mathbb{O}^{(0)}$ and $\mathbb{S}^{(0)}$ are the vorticity and strain of the fluid velocity field at $\boldsymbol{x}(t)$ and time t. Hence, straining regions, where $\mathrm{Tr}\mathbb{S}\mathbb{S}^T > \mathrm{Tr}\mathbb{O}\mathbb{O}^T$, are sinks of the particle velocity field while regions of high vorticity act as sources. As a result, weakly inertial particles tend to accumulate in straining regions of the flow in accordance with the intuitive picture discussed earlier [1]. Note that the result (2.3) suggests that the effect of preferential concentration is proportional to the Kubo number. This is intuitively clear recalling that Ku measures the persistence of the flow. In a memoryless flow with $\mathrm{Ku} \to 0$, the aerosol particles react too slowly to changes of the flow as to be able to accumulate in straining regions.

A conceptual problem with perturbative expansions of this kind is that the representation of the particle velocity field as a simple function of the smooth flow fields $\mathbb{A}^{(i)}(t)$ explicitly excludes particle-trajectory crossings. These crossings become relevant for larger St numbers and appear due to caustics in the particle phase-space dynamics. We discuss caustics in Section 2.1.3.

2.1.2 Phase-space contraction

The equations of motion governing the particle motion in aerosols are dissipative, which means that energy brought into the system eventually leaves it again. Dissipative systems have the property that their phase space volume decreases with time [31]. Consider the equations of motion in Kubo coordinates, Eq. (2.1). Phase-space contraction is quantified by the divergence of the flow, $\mathrm{div}[(\dot{\boldsymbol{x}}(t), \dot{\boldsymbol{v}}(t))]$, taken with respect to the pair $(\boldsymbol{x}(t), \boldsymbol{v}(t))$. We obtain

$$\mathrm{div}[(\dot{\boldsymbol{x}}(t), \dot{\boldsymbol{v}}(t))] = \mathrm{Ku} \sum_{i=1}^{d} \frac{\partial v_i(t)}{\partial x_i(t)} + \frac{1}{\mathrm{St}} \sum_{i=1}^{d} \left(\frac{\partial u_i(\boldsymbol{x}(t), t)}{\partial v_i(t)} - \frac{\partial v_i(t)}{\partial v_i(t)} \right) = -\frac{d}{\mathrm{St}} < 0 \,. \quad (2.4)$$

First, we observe that the divergence of the flow is negative and independent of the coordinates and of time. It follows that phase space volumes $\mathscr{W}_t$ evolve according to

$$\mathscr{W}_t = \mathscr{W}_{t_0} \mathrm{e}^{\int_{t_0}^{t} \mathrm{div}[(\dot{\boldsymbol{x}}(t), \dot{\boldsymbol{v}}(t))] \mathrm{d}t} = \mathscr{W}_{t_0} \mathrm{e}^{-\frac{d}{\mathrm{St}}(t - t_0)} \,. \quad (2.5)$$

Thus phase space volumes contract exponentially. The same is true for *spatial* volumes of particles $\mathscr{V}_t = \det \mathbb{J}(t)$ that evolve according to the flow

(2.1), due to a related phenomenon called multiplicative amplification [1]. Multiplicative amplification and phase-space contraction are naturally described by means of Lyapunov exponents [1, 45, 47], which we discuss in Section 2.2.2.

2.1.3 Caustics

Another mechanism that we know is relevant for spatial clustering is the occurrence of caustics [6, 7, 8, 15]. Caustics are singularities in the projection of the phase-space manifold on the coordinate space. Roughly speaking, because the dynamics of inertial particles takes place in $2d$ dimensional phase space, both the particle field $\boldsymbol{x}(\boldsymbol{x}_0, t)$ and its corresponding velocity field $\boldsymbol{v}(\boldsymbol{x}(t), t)$ are in general multivalued functions with respect to the d-dimensional coordinate space. Caustics have important consequences for the particle distribution. At the 'caustic lines', the tangent space of the phase-space manifold is perpendicular to the coordinate space. This implies that the particle density diverges in a square-root fashion and the probability of finding particles close to each other is strongly increased at the caustic lines [7]. The left panel in Fig. 2.2 shows caustic lines for inertial particles (in red) in a two-dimensional random flow. The right panel depicts schematically how a caustic line is created at the point x_c, where $\partial v(x,t)/\partial x$ diverges. In addition to its importance for spatial clustering, the multi-valuedness of the particle field also allows for large relative velocities between nearby particles [6, 7, 8]. For this reason, some authors call the occurrence of caustics the 'sling effect' [6, 15]: Particles may be strongly accelerated in different regions in space to come together at high relative velocity. Locally, we can define a caustic as the event that the Jacobian of the particle field $\mathbb{J}(t)$ becomes singular at finite time t_c:

$$\det \mathbb{J}(t_c) = 0\,. \tag{2.6}$$

This is equivalent to saying that the volume of the spatial parallelepiped spanned by nearby particles collapses to zero [1]. We can express this condition in terms of $\mathbb{Z}(t)$ by taking a time-derivative of $\det \mathbb{J}(t)$ and using the equation of motion (2.1c). We obtain

$$\tfrac{\mathrm{d}}{\mathrm{d}t} \det \mathbb{J}(t) = \det \mathbb{J}_t \operatorname{Tr}\left[\mathbb{J}^{-1}\dot{\mathbb{J}}\right] = \mathrm{Ku} \det \mathbb{J}(t) \operatorname{Tr} \mathbb{Z}(t)\,. \tag{2.7}$$

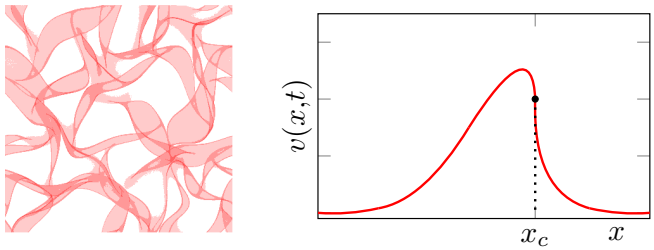

Figure 2.2: *Left:* Distribution of inertial particles in a two dimensional random flow. Caustic lines are the dark-red regions of high particle density. The figure is taken from [1] with permission. *Right:* One-dimensional schematic of the creation of a caustic at x_c.

Because $\mathbb{J}(t_0) = \mathbb{1}$ we find for $\det \mathbb{J}(t)$ as a function of $\mathbb{Z}(t)$ [1]

$$\det \mathbb{J}(t) = \mathrm{e}^{\mathrm{Ku}\int_{t_0}^{t} \mathrm{Tr}\,\mathbb{Z}(s)\mathrm{d}s}, \tag{2.8}$$

which implies that the event of caustic formation can be expressed as

$$\int_{t_0}^{t_c} \mathrm{Tr}\,\mathbb{Z}(s)\mathrm{d}s \to -\infty, \tag{2.9}$$

at finite time $t_c < \infty$.

2.1.4 Compressibility of the underlying flow

Because the models that we discuss in Chapters 3 are one-dimensional, their underlying flow must be compressible. A compressible flow leads to strong clustering of the immersed particles. This is true even for tracer particles with $\mathrm{St} = 0$, which can be seen by taking the trace of Eq. (2.2). We have

$$\mathrm{Tr}\,\mathbb{Z}(t) = \nabla \cdot \boldsymbol{v}(t) \sim \mathrm{Tr}\,\mathbb{A}^{(0)}(t) = \nabla \cdot \boldsymbol{u}(\boldsymbol{x}^{(0)}(t), t), \tag{2.10}$$

to lowest order in the Stokes number. Recall that $\boldsymbol{x}^{(0)}(t)$ is the field of inertialess tracer particles. Consequently, coordinate space volumes, which are measured by $\det \mathbb{J}(t)$, shrink at sinks where $\nabla \cdot \boldsymbol{u}(\boldsymbol{x}(t), t) < 0$. For weak inertia, clustering that is due to the compressibility of the underlying flow is characterised by a 'path-coalescence' regime [16] in which the phase-space manifold contracts to a point. For larger Stokes numbers, a phase transition

occurs and the particles behave essentially as in an incompressible flow [16, 48]. This 'path-coalescence transition' [16] is discussed in more detail in Section 3.3.2 for one-dimensional statistical models.

2.2 Quantities that characterise spatial clustering

We now discuss three different observables that measure clustering in different ways. These are the spectrum of fractal dimensions D_q, the statistics of the finite-time Lyapunov exponents λ_t and the rate of caustic formation J.

2.2.1 Fractal dimension spectrum

Spatial clustering is characterised by inhomogeneities in the spatial distribution of aerosol particles [1, 13, 14, 30]. One way of characterising these inhomogeneities is by calculating the fractal dimension spectrum [12, 49, 50].

In order to define the most intuitive representative of the spectrum, the 'box-counting' dimension D_0, we discretise the space into small boxes of side length $\epsilon \ll 1$ and consider a large but finite number $N \gg 1$ of particles. For a homogeneous particle distribution, the expected minimum number of boxes $\langle \mathcal{N}(\epsilon) \rangle$ of side length ϵ needed to cover the set $\mathcal{S}$ of N particles scales as the box-size raised to the power $-d$, $\langle \mathcal{N}(\epsilon) \rangle \sim \epsilon^{-d}$. If the particle density is non-homogeneous, less boxes are needed and the scaling exponent is smaller than d. The box-counting dimension D_0 is defined by [51]

$$\langle \mathcal{N}(\epsilon) \rangle \sim \epsilon^{-D_0}, \quad \epsilon \ll 1. \tag{2.11}$$

The box-counting dimension measures, roughly speaking, how space-filling a fractal is [51, 52]. In many cases, in particular if a fractal is generated by a set of underlying equations of motion, it is furthermore equipped with a non-trivial measure, called the natural measure μ [31]. The latter contains information not only about *if* regions on the fractal are visited by the particles but also *how often* that happens. In order to study the natural measure on the fractal, we consider the probability $\mu(\boldsymbol{x}(t), \epsilon)$ that a sphere of radius ϵ centered at $\boldsymbol{x}(t)$ is visited by a particle. The spectrum of fractal dimensions D_q is defined in terms of the scaling relation [52]

$$\left\langle \int_{\mathcal{S}_t} \mu(\boldsymbol{x}(t), \epsilon)^{q-1} \mathrm{d}\mu(\boldsymbol{x}(t), \epsilon) \right\rangle \sim \epsilon^{(q-1)D_q}, \quad \epsilon \ll 1. \tag{2.12}$$

The integral is performed over the fractal set $\mathscr{S}_t$ at time t and the bracket $\langle\cdot\rangle$ denotes a time average. The quantity D_q is called Rényi dimension or generalised fractal dimension [52]. From Eq. (2.12) we obtain

$$D_q = \lim_{\epsilon\to 0} \frac{1}{q-1} \frac{\log\left\langle \int_{\mathscr{S}_t} \mu(\boldsymbol{x}(t),\epsilon)^{q-1} \mathrm{d}\mu(\boldsymbol{x}(t),\epsilon)\right\rangle}{\log\epsilon}. \tag{2.13}$$

The most important fractal dimension in the present context is the correlation dimension, D_2 [13, 53, 54]. Setting $q=2$ in Eq. (2.13) we obtain

$$D_2 = \lim_{\epsilon\to 0} \frac{\left\langle \int_{\mathscr{S}_t} \mu(\boldsymbol{x}(t),\epsilon) \mathrm{d}\mu(\boldsymbol{x}(t),\epsilon)\right\rangle}{\log\epsilon}. \tag{2.14}$$

The correlation dimension is of great importance for physical particle systems, because it measures the probability of finding a second particle in a ball of radius ϵ around a reference particle [55]. That is why a convenient way of formulating Eq. (2.14), is by considering the statistics of separations of a particle pair, $Y^{(2)}(t) = \|\boldsymbol{x}_1(t) - \boldsymbol{x}_2(t)\|$. For this quantity it follows from Eq. (2.12) that [52]

$$P(Y^{(2)}(t) \le \epsilon) \sim \epsilon^{D_2}, \qquad \epsilon \ll 1. \tag{2.15}$$

More generally, consider the positions of $q \ge 2$ particles $\boldsymbol{x}_i(t)$, $i = 1,\ldots,q$, and define the quantity

$$Y^{(q)}(t) = \max_{i,j\in S_q} \{\|\boldsymbol{x}_i(t) - \boldsymbol{x}_j(t)\|\}, \tag{2.16}$$

where S_q denotes the index set $S_q = \{1,\ldots,q\}$. It can be shown [12, 52] that $Y^{(q)}(t)$ obeys the scaling relation

$$P(Y^{(q)}(t) \le \epsilon) \sim \epsilon^{D_q(q-1)}, \qquad \epsilon \ll 1, \tag{2.17}$$

for $q \ge 2$. In the majority of this work, we study the correlation dimension D_2. The other fractal dimensions are studied for $q > 2$ in paper C, where a simple relation between the different fractal dimensions is found for a particular model.

2.2.2 Finite-time Lyapunov exponents

The relative spatial dynamics of nearby particles is characterised by stretching and folding due to the random fluid velocity gradients. The transients of these deformations are important for clustering and are described by the spatial finite-time Lyapunov exponents (FTLE) [1, 12, 18, 26, 45]. The spatial FTLE are obtained from the eigenvalues of $\mathbb{J}(t)$, which we call $\Lambda_k(t)$ with $k = 1,\dots,d$. In the limit $t \to \infty$, the absolute values of these multipliers, $|\Lambda_k(t)|$, typically scale exponentially with characteristic (Lyapunov) exponent λ_k. For large enough but finite times, the $|\Lambda_k(t)|$ are stochastic processes with exponents $\lambda_k(t)$:

$$|\Lambda_k(t)| \sim \mathrm{e}^{\lambda_k(t)t}, \quad k = 1,\dots,d\,. \tag{2.18}$$

The processes $\lambda_k(t)$ are called the spatial finite-time Lyapunov exponents (FTLE) of the system [26, 56]. The spatial FTLE approach the spatial Lyapunov exponents in the limit $t \to \infty$, $\lambda_k(t) \to \lambda_k$. In terms of the multipliers $\Lambda_k(t)$, the FTLE are expressed as $\lambda_k(t) = t^{-1}\log|\Lambda_k(t)|$. Furthermore, using Eqs. (2.8) and (2.18) we obtain

$$\sum_{k=1}^{d}\lambda_k(t) = \frac{\mathrm{Ku}}{t}\int_0^t \mathrm{Tr}\,\mathbb{Z}(t)\,\mathrm{d}t\,. \tag{2.19}$$

In the infinite-time limit we can thus find a simple expression for the sum of spatial Lyapunov exponents according to

$$\sum_{k=1}^{d}\lambda_k = \lim_{t\to\infty}\frac{\mathrm{Ku}}{t}\int_0^t \mathrm{Tr}\,\mathbb{Z}(t)\,\mathrm{d}t = \mathrm{Ku}\,\langle \mathrm{Tr}\,\mathbb{Z}\rangle\,, \tag{2.20}$$

where the the expectation value in the last equality is taken with respect to the natural measure of the dynamics.

The model systems in Chapter 3 are all one-dimensional, $d = 1$, so that Eqs. (2.19) and (2.20) in fact are expressions for the only spatial FTLE and Lyapunov exponent of the theory, respectively. That is why these equations are particularly important here. In systems with $d > 1$, the sum of all spatial Lyapunov exponents describes how spatial volumes expand ($\sum_{k=1}^{d}\lambda_k > 0$) or contract ($\sum_{k=1}^{d}\lambda_k < 0$). For a complete description of local stretching and compression, however, the whole set of Lyapunov exponents is required.

In Section 2.1.2 we noted that phase-space volumes $\mathcal{W}_t$ of particles tend to contract under the flow at a constant exponential rate. In terms of the Lyapunov exponents Eq. (2.5) implies that the sum of all phase-space Lyapunov exponents sums up to $-d/\mathrm{St}$.

The statistics of the spatial FTLE is studied in terms of their joint probability density function $P(\boldsymbol{\lambda}(t)=\boldsymbol{s})$ where $\boldsymbol{\lambda}(t)=(\lambda_1(t),\ldots,\lambda_d(t))$. For large times, $t\gg 1$, $P(\boldsymbol{\lambda}(t)=\boldsymbol{s})$ takes the large deviation form [57]

$$P(\boldsymbol{\lambda}(t)=\boldsymbol{s})\approx \exp\left[-t\,I(\boldsymbol{s})\right], \qquad t\gg 1, \tag{2.21}$$

where $I(\boldsymbol{s})$ is called the rate function of the process $\boldsymbol{\lambda}(t)$. In one dimension, $d=1$, there is a simple relation between the rate function for the FTLE and the correlation dimension of the system that is discussed in Chapter 3 and Appendix A.

2.2.3 Rate of caustic formation

In Section 2.1.3 we showed that a caustic forms when the integral $\int_{t_0}^{t_c}\mathrm{Tr}\,\mathbb{Z}(s)\mathrm{d}s$ tends to $-\infty$ in finite time $t_c<\infty$. Similarly to the FTLEs discussed in the previous section we treat t_c as a random variable. We call t_i the time between the i^{th} and $(i-1)^{\text{th}}$ caustic event. The number $N(t)$ of caustics that have occurred at time $t>0$ can then be written as

$$N(t):=\max\{n: T_n\le t\}, \tag{2.22}$$

where $T_n=\sum_{i=1}^{n}t_i$. For systems with sufficiently quickly decaying correlation functions, we may assume ergodicity so that $N(t)$ constitutes a so-called renewal process [58]. For renewal processes one can prove that [58]

$$\frac{N(t)}{t}\to\frac{1}{\langle t_i\rangle}, \qquad \text{for} \qquad t\to\infty. \tag{2.23}$$

We call the limit in this equation J, the rate of caustic formation

$$J=\frac{1}{\langle t_i\rangle}=\lim_{t\to\infty}\frac{N(t)}{t}. \tag{2.24}$$

The rate of caustic formation is a measure for the importance of caustics for spatial clustering in a given system. Typically, caustics are negligible against

the other clustering mechanisms when Ku and/or St are small. In this case, J shows an exponentially small activation of the type [1, 7, 8, 15]

$$J \sim \mathrm{e}^{-1/f(\mathrm{Ku},\mathrm{St})}, \tag{2.25}$$

where f is a function Ku and St. The explicit form of f is known analytically only for one-dimensional models in specific limits of Ku and St [7, 43]. We discuss these results in Section 3.4.1.

3 One-dimensional systems

In this Chapter we introduce the one-dimensional statistical models, which we use to study the observables defined in the previous Chapter. In one spatial dimension, the statistical model is much simpler than in two and three dimensions and allows for analytical treatment in limiting cases. The equations of motion in Kubo coordinates, Eq. (1.21), read in one dimension:

$$\frac{\mathrm{d}}{\mathrm{d}t}x(t) = \mathrm{Ku}\, v(t), \tag{3.1a}$$

$$\frac{\mathrm{d}}{\mathrm{d}t}v(t) = \mathrm{St}^{-1}\left[u(\boldsymbol{x}(t),t) - v(t)\right], \tag{3.1b}$$

$$\frac{\mathrm{d}}{\mathrm{d}t}j(t) = \mathrm{Ku}\, z(t) j(t), \tag{3.1c}$$

$$\frac{\mathrm{d}}{\mathrm{d}t}z(t) = \mathrm{St}^{-1}\left[A(x(t),t) - z(t)\right] - \mathrm{Ku}\, z(t)^2. \tag{3.1d}$$

Note that all field quantities are now scalars. The one-dimensional matrix of spatial deformations, $j(t) = \partial x(x_0,t)/\partial x_0$ can alternatively be described by the separation $|\Delta x(t)| = |x_1(t) - x_2(t)|$ of a closeby particle pair which has the same dynamics as $j(t)$ [1].

We now briefly discuss the implications of reduced dimensionality for the calculation of the observables discussed in Section 2.2. We start by considering the computation of the spatial FTLE. Because there is only one spatial FTLE in one dimension, Eq. (2.19) turns into the simple equation

$$\lambda(t) = \frac{1}{t}\int_0^t z(s)\mathrm{d}s\,. \tag{3.2a}$$

Consequently, from Eq. (2.20) we get for the Lyapunov exponent

$$\lambda = \lim_{t\to\infty}\lambda(t) = \langle z\rangle\,. \tag{3.3}$$

Eq. (2.9) translates into the one-dimensional caustic condition

$$\int_0^{t_c} z(s)\mathrm{d}s \to -\infty\,. \tag{3.4}$$

3.1 Generic behaviour

Equation (3.4) implies that a necessary condition for caustic formation is that $z(t) \to -\infty$ in finite time. In one dimension, this means that the dynamics of

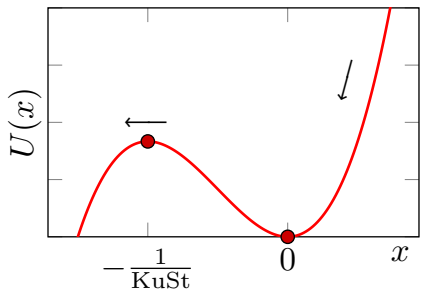

Figure 3.1: The z-coordinate moves in the potential $U(x)$, leading to a finite flux towards $z=-\infty$.

$z(t)$ needs to exhibit finite-time singularities. How these caustic singularities arise becomes clear by writing Eq. (3.1d) as

$$\frac{\mathrm{d}}{\mathrm{d}t}z(t) = -U'(z(t)) + \mathrm{St}^{-1}A(t), \tag{3.5}$$

with the potential $U(x) = \frac{\mathrm{St}^{-1}}{2}x^2 + \frac{\mathrm{Ku}}{3}x^3$. Figure 3.1 schematically shows U as a function of x. If we disregard for the moment the contribution of $A(t)$, the z-dynamics $U(x)$ has a stable fixed point at $x=0$ and an unstable one at $x=-1/(\mathrm{KuSt})$ [1]. The fixed points are shown as the red dots in Fig. 3.1. For finite and large enough values of $A(t)$, the z-coordinate can pass the unstable fixed point and escape to $-\infty$ [6, 16]. A closer analysis of the equation of motion (3.1d) shows that the singularity $z \to -\infty$ is reached in finite time and is not integrable, thus leading to a caustic by Eq. (3.4). We know from Eq. (2.8) that $j(t)$ goes to zero at a caustic, $j(t_c)=0$. For $t > t_c$, $j(t)$ must become positive again which requires that $z(t)$ is, immediately after a caustic, injected back at $+\infty$.

We conclude that $z(t)$ obeys the following dynamics: For small $A(t)$, the z-coordinate spends most of its time close to the origin. When $A(t)$ becomes larger it is more likely that $z(t)$ passes the unstable fixed point at $z=-1/(\mathrm{KuSt})$ and escapes to $-\infty$. Due to the periodic boundary conditions $z(t)$ eventually returns to the origin $z=0$ after a caustic event. Hence, after a long enough time, $z(t)$ reaches a non-equilibrium steady state characterised by a constant negative flux.

3.2 Statistical models in one dimension

In one dimension the Fourier sum (1.4) for $u(x,t)$ discussed in Section 1.5, reads in Kubo coordinates

$$u(x,t) = \partial_x \phi(x,t) = N \sum_{k=-\infty}^{\infty} ik\, a_k(t) \mathrm{e}^{ikx - k^2/4}, \tag{3.6}$$

where $N = \left(\sqrt{2\pi}\eta/L\right)^{1/2}$. Recall that $a_k(t)$ are chosen to be independent Ornstein-Uhlenbeck processes. Consequently, $A(x,t) = \partial_x u(x,t)$ is a Gaussian random field with zero mean and correlation

$$\langle A(x,t)A(y,s)\rangle = \left\{[(x-y)^2-3]^2-6\right\} \mathrm{e}^{-(x-y)^2/2} \mathrm{e}^{-|t-s|}. \tag{3.7}$$

The model is applicable to the whole range of both Ku and St but it is hard to obtain analytical results for it, even in one spatial dimension. In what follows, we introduce three versions of the statistical model for which analytical results can be obtained.

3.2.1 White-noise model

The white-noise model is obtained by using the equations of motion is Stokes coordinates, Eq. (1.21), and simultaneously letting $\mathrm{Ku} \to 0$ and $\mathrm{St} \to \infty$ so that $\varepsilon^2 = 3\mathrm{Ku}^2\mathrm{St}$ remains constant. In the white-noise limit, the correlation function turns into a delta function in time:

$$\langle A(x,t)A(y,s)\rangle \to 2\varepsilon^2 \left\{[(x-y)^2-3]^2-6\right\} \mathrm{e}^{-(x-y)^2/2} \delta(t-s). \tag{3.8}$$

Because the particles move too slowly compared to the flow to accumulate in straining regions, there is no preferential concentration in the white-noise model. Hence, the random field $A(x,t)$ at fixed x has the same statistics as $A(x(t),t)$, which means in turn that $A(t) = \xi_t$, where ξ_t is a Gaussian white-noise [59, 60] with correlation

$$\langle \xi_t \xi_s \rangle = 2\varepsilon^2 \delta(t-s). \tag{3.9}$$

The equations of motion for $j(t)$ and $z(t)$ read in the white-noise model

$$\tfrac{\mathrm{d}}{\mathrm{d}t} x(t) = z(t)x(t), \tag{3.10a}$$

$$\tfrac{\mathrm{d}}{\mathrm{d}t} z(t) = \xi_t - z(t) - z^2(t). \tag{3.10b}$$

Modelling $A(t)$ by the Gaussian white-noise ξ_t corresponds to the physical situation of highly inertial particles ($\mathrm{St}\to\infty$) in a very quickly varying flow ($\mathrm{Ku}\to 0$). The set of stochastic differential equations given in Eqns. (3.10) constitutes a Markov system which can be treated using Fokker-Planck equations [59, 60]. This is one of the reasons why the white-noise model has been studied extensively in one [1, 10, 61, 62] and higher dimensions [47, 53, 54, 63].

3.2.2 Telegraph model

In the so-called telegraph model [17] the velocity gradient $A(t)$ is modelled by a telegraph process η_t. The latter is a jump process that takes only two different values, A_0 and $-A_0$, where $A_0>0$ is the amplitude of the process. Transitions from A_0 to $-A_0$ occur with rate ν_- and back from $-A_0$ to A_0 with rate ν_+. For large times, η_t reaches a steady state characterised by the probabilities

$$\lim_{t\to\infty} P\left(\eta_t = A_0\right) = \frac{\nu_+}{\nu}, \qquad \lim_{t\to\infty} P\left(\eta_t = -A_0\right) = \frac{\nu_-}{\nu}, \tag{3.11a}$$

where we denote $\nu \equiv \nu_+ + \nu_-$. The mean value $\mu = \langle \eta_t \rangle$ and correlation function $\langle\!\langle \eta_t \eta_s \rangle\!\rangle = \langle \eta_t \eta_s \rangle - \langle \eta_t \rangle \langle \eta_s \rangle$ for the telegraph process can be obtained explicitly [60]. The steady-state correlation function takes the simple form

$$\langle\!\langle \eta_t \eta_s \rangle\!\rangle = \left(A_0^2 - \mu^2\right) \mathrm{e}^{-\nu|t-s|}. \tag{3.12}$$

Comparing Eq. (3.12), to Eq. (3.7) we observe that we can parametrise the telegraph model in terms of Ku, St and μ if we identify

$$\nu = \mathrm{St}, \qquad 3\mathrm{Ku}^2\mathrm{St}^2 = A_0^2 - \mu^2. \tag{3.13}$$

Closer inspection of the model [17], reveals that in order for the combined process $(j(t), z(t), \eta_t)$ to be stationary, one needs to define μ as a function of the parameters Ku and St. One possible and consistent choice is to fix μ to be the negative root[1] of the quadratic equation [17]

$$\mu^2 + \mu\mathrm{St}(\mathrm{St}+1) + 3\mathrm{Ku}^2\mathrm{St}^2 = 0. \tag{3.14}$$

Thus $\langle A(x(t),t)\rangle = \langle \eta_t \rangle = \mu < 0$ even though $\langle A(x,t)\rangle = 0$ for all x. Hence, the consistency condition (3.14) introduces preferential sampling of negative

[1] The model corresponding to the positive root turns out to be unphysical.

fluid gradients in the model [17]. The quadratic equation (3.14) has real solutions for μ as long as

$$\mathrm{Ku} \leq (\mathrm{St}+1)/\sqrt{12}\,, \tag{3.15}$$

which prescribes the regime of applicability of the model. The telegraph model has several interesting properties. Apart from being mathematically tractable, the model exhibits a region in (Ku, St) state space, where no caustics occur, because the noise η_t is bounded [17]. Further, the telegraph process turns into the Gaussian white-noise for $\mathrm{St} \to \infty$ and $\mathrm{Ku} \to 0$ if $\mathrm{Ku}^2\mathrm{St} = \varepsilon^2/3$ remains constant. In this sense, it is a generalisation of the white-noise model discussed in Section 3.2.1, with finite correlation time.

3.2.3 Persistent-flow model

The persistent-flow model is another limit of the statistical model that we have come across recently. We discuss the results for this model only briefly in this Chapter and leave details to a future publication. The model is obtained by taking $\mathrm{Ku} \to \infty$ and $\mathrm{St} \to 0$ such that $\mathrm{Ku}^2\mathrm{St}^2 = \kappa^2/3$ remains constant [1]. Physically, this limit describes a situation in which the flow persists for many relaxation times of the particle dynamics [61]. The particles at each instance in time adapt to the adiabatic changes of the flow field. In this limit, the correlation function for $A(x,t)$ in Stokes coordinates turns into

$$\langle A(x,t)A(y,s)\rangle \to 3\kappa^2\left\{[(x-y)^2-3]^2-6\right\}\mathrm{e}^{-(x-y)^2/2}\,. \tag{3.16}$$

Note that the exponential time correlation is constant in this limit, $\mathrm{e}^{-\mathrm{St}|t-s|} \to 1$ and the flow field loses its time dynamics. The Gaussian statistics of $A(x,t)$ is obtained from averaging over different realisations of the flow. Because changes of the flow field are infinitely slow, there is strong preferential sampling of negative fluid velocity gradients. Obtaining realistic but non-trivial statistics for $A(x(t),t)$ in the persistent-flow model is a non-trivial task. Naively, particles in a highly persistent flow accumulate at those zeros of $u(x,t)$ at which the corresponding gradients $A(x,t)$ are negative. For Gaussian random functions, the distribution of these gradients is given by the Kac-Rice formula for random functions [64, 65, 66]. If we call $\bar{A} = \lim_{t\to\infty} A(x(t),t)$, the statistics of gradients according to the Kac-Rice formula reads [66]

$$P(\bar{A}=a) = \frac{|a|}{\kappa^2}\mathrm{e}^{-a^2/(2\kappa^2)}\theta(-a)\,. \tag{3.17}$$

Trivially, the gradient statistics in Eq. (3.17) forbids positive gradients $P(\bar{A} > 0) = 0$. The correlation function is given by

$$\lim_{t,s\to\infty} \langle\!\langle A(x(t),t)A(x(s),s)\rangle\!\rangle = \langle \bar{A}^2\rangle - \langle \bar{A}\rangle^2 = 2\kappa^2 \,. \tag{3.18}$$

A naive application of the Kac-Rice statistics does, however, not include the following dynamical effect [67]: Even if $u(x,t)$ changes its shape very slowly, zeros of $u(x,t)$ can still appear and disappear at a low but finite rate. Whenever a stable zero of $u(x,t)$ disappears, the particles that were trapped there need to travel to the next stable zero and sample non-negative flow gradients on their way [67]. Including this effect leads to a non-vanishing probability of positive gradients, $P(\bar{A} > 0) > 0$, in contradiction to the Kac-Rice statistics (3.17). This more sophisticated approach is ongoing work. As a proof of concept, we describe here the case of a Gaussian density but with mean $\langle \bar{A} \rangle$ and variance $\langle\!\langle \bar{A}^2 \rangle\!\rangle$ adjusted to the Kac-Rice statistics (3.17). We believe this distribution has similar properties as the realistic density including the aforementioned dynamical effect. Our density $P(\bar{A} = a)$ thus reads

$$P(\bar{A} = a) = \frac{\mathrm{e}^{-\frac{(a-\langle \bar{A}\rangle)^2}{4\kappa^2}}}{\sqrt{4\pi\kappa^2}} \,. \tag{3.19}$$

with mean and variance

$$\langle \bar{A}\rangle = -\sqrt{\frac{\pi}{2}}\kappa \,, \qquad \langle\!\langle \bar{A}^2\rangle\!\rangle = 2\kappa^2 \,. \tag{3.20}$$

Because $\bar{A}$ is treated as a constant in the equation of motion for $z(t)$, the model is exactly solvable, independent of the chosen statistics of $\bar{A}$.

3.3 Observables

In this Section, we compute the observables defined in Section 2.2 in terms of the three models discussed above.

3.3.1 Probability distributions

In all three models, the z-coordinate has a statistical steady state distribution with a finite negative flux, given by the rate of caustic formation. For the

white-noise model, this distribution is obtained from the Fokker-Planck equation corresponding to the white-noise equation of motion (3.10). We have [1]

$$P(z(t)=z)=\frac{J}{\varepsilon^2}\mathrm{e}^{-U(z)/\varepsilon^2}\int_{-\infty}^{z}\mathrm{e}^{U(t)/\varepsilon^2}\mathrm{d}t\,, \tag{3.21}$$

with $U(x)=x^2/2+x^3/3$ and J given by

$$J^{-1}=\int_{-\infty}^{\infty}\mathrm{e}^{-U(s)/\varepsilon^2}\int_{-\infty}^{s}\mathrm{e}^{U(t)/\varepsilon^2}\mathrm{d}t\,\mathrm{d}s\,. \tag{3.22}$$

The distribution $P(z(t)=z)$ has power-law tails for $|z|\to\infty$. These are due to the events that the $z(t)$ coordinate escapes to $-\infty$. Indeed, the weight of the tails for large z is directly proportional to the rate of caustic formation J according to

$$P(z(t)=z)\sim\frac{J(\varepsilon)}{z+z^2}\,,\qquad |z|\to\infty\,. \tag{3.23}$$

The same asymptotic relation holds true for both the telegraph and the persistent-flow model, only replacing $J(\varepsilon)$ in Eq. (3.23) by $J(\mathrm{Ku},\mathrm{St})$ and $J(\kappa)$, respectively. The derivation of the densities varies, however, since the Fokker-Planck equation can be used only in the white-noise model. For the telegraph model $P(z(t)=z)$ can be obtained from the 'Formula of differentiation' [68] which was done in Ref. [17]. In the persistent-flow model the conditional distribution $P(z(t)=z|\bar{A}=a)$ is computed for constant $A(t)=\bar{A}$. Then one uses

$$P(z(t)=z)=\int_{\mathbb{R}}P(z(t)=z|\bar{A}=a)P(\bar{A}=a)\mathrm{d}a\,, \tag{3.24}$$

and Eq. (3.19) to obtain the distribution function. Figure 3.2 shows the distributions $P(z(t)=z)$ for the three different models, the white-noise model, the telegraph model and the persistent-flow model, in the left, middle and right panels, respectively. All distributions have been obtained analytically using the methods outlined above. The dashed lines show the corresponding asymptotics (3.23) which agree well with the densities at large z. The expressions for the rate of caustic formation that enter in Eq. (3.23) were obtained analytically in terms of integrals similar to Eq. (3.22), but are not shown here. Note that for the telegraph model, two different distributions are shown in the middle panel of Fig. 3.2, one for small St and large Ku (light

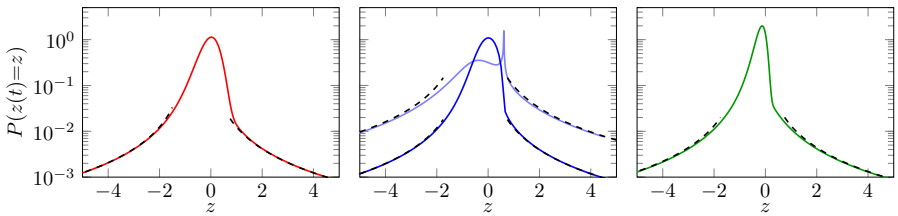

Figure 3.2: *Left:* Steady-state distribution $P(z(t) = z)$ for the white-noise model obtained from Eq. (3.21) with $\varepsilon^2 = 0.1$ (red) and the asymptotics (3.23) (black dashed). *Middle:* Distributions obtained from the telegraph model with $(\mathrm{Ku}, \mathrm{St}) = (0.5, 1.0)$ (light blue) and $(\mathrm{Ku}, \mathrm{St}) = (0.0577, 10)$ (dark blue). *Right:* Distribution obtained from the persistent-flow model with $\kappa = 0.1$.

blue) and the other one for small Ku and large St. The exact values for (Ku, St) are given in the Figure text. For large Ku and small St, the density develops an integrable singularity at the stable fixed point, which is absent in the other models [17]. The probability distributions depend surprisingly little on the choice of model. This can be understood phenomenologically by returning to the picture of the escape from the stable fixed point discussed in Section 3.1: The main ingredients that shape the z-distribution are given by the attraction towards the stable fixed point on the one hand and the escape process with subsequent return on the other hand. While the former shapes the maximum around the origin, the latter leads to the power-law tails.

3.3.2 Lyapunov exponent

A compressible underlying flow leads to strong particle clustering indicated by a negative spatial Lyapunov exponent, $\lambda < 0$. The Lyapunov exponent for the models is calculated from Eq. (3.3) using the z-distributions obtained in the previous Section. In all three models we consider in this work, the Lyapunov exponent is negative at small inertia parameter. A negative Lyapunov exponent implies that all paths in the particle dynamics eventually coalesce, which is the strongest form of clustering. For larger inertia, the Lyapunov exponent becomes positive [16]. This behaviour is known for the white-noise model [16, 48], the telegraph model [17] and can also be observed in the persistent-flow model. The left panel in Fig. 3.3 shows the Lyapunov exponents for the white-noise model (red curve) as a function of ε^2 as well as for the persistent-flow model (green curve) as a function of κ. The path-

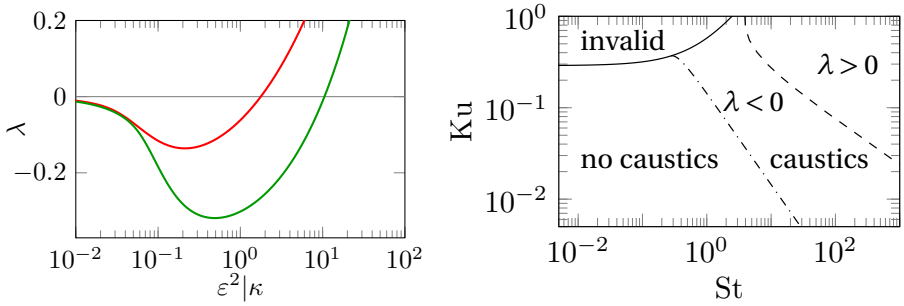

Figure 3.3: *Left:* Lyapunov exponent in the white-noise model (red) and for the persistent-flow model (green) as functions of the respective inertia parameters ε^2 and κ. *Right:* Phase diagram for the telegraph model in the (Ku, St) plane.

coalescence transition occurs at $\varepsilon \approx 1.33$ and $\kappa \approx 10.42$ for the white-noise and persistent-flow models, respectively. The right panel shows the more intricate phase diagram of the telegraph model [17] in the (Ku, St) plane. The black dashed line indicates the location of the path coalescence transition. The dash-dotted line separates the phase where caustics occur from that where caustics are absent. The solid black line defines the regime of validity according to Eq. (3.15).

3.3.3 Finite-time Lyapunov exponents

In this Section, we discuss how the statistics of the FTLE is obtained for the white-noise and the persistent-flow model. We leave out the telegraph model from the discussion, because we have not been able to obtain sufficiently accurate results for it yet. We determine the rate function $I(s)$ for the FTLE by Legendre transform of the corresponding scaled cumulant generating function $G_s(k)$ [57]. The latter is defined by

$$G_s(k) = \lim_{t\to\infty} \frac{1}{t} \log\langle e^{k\,t\,\lambda(t)}\rangle = \lim_{t\to\infty} \frac{1}{t} \log\langle j(t)^k\rangle\,. \tag{3.25}$$

The rate function $I(s)$ is given by the Legendre transform of $G_s(k)$ [69, 70]

$$I(s) = \sup_{k\in\mathbb{R}} [k\,s - G_s(k)]\,. \tag{3.26}$$

Hence, our task is to calculate the scaled cumulant generating function. For the persistent-flow model, it can obtained analytically by means of an

integral, that we do not show here. In the white-noise model, the cumulant generating function is obtained as the largest eigenvalue $\zeta^{\max}(k) = G_s(k)$ of a differential operator, the so-called tilted generator $\mathscr{L}_k$ [57, 71], which depends on the parameter k. The tilted generator for the FTLE is given by [71]

$$\mathscr{L}_k = \mathscr{L} + kz\,, \quad \text{with} \quad \mathscr{L} = \partial_z\big[z + z^2 + \varepsilon^2\partial_z\big]\,. \tag{3.27}$$

Note that for $k = 0$ the $\mathscr{L}_k$ reduces to the Fokker-Planck operator $\mathscr{L}$ corresponding to Eq. (3.10b). For small ε the largest eigenvalue $\zeta^{\max}(k)$ can be calculated from Eq. (3.27) in perturbation theory. One finds

$$G_s(k) \sim \varepsilon^2 k(k-1)\big[1 + (5-4k)\varepsilon^2 + \big(32k^2 - 86k + 60\big)\varepsilon^4 + \big(-336k^3 + 1437k^2 - 2135k + 1105\big)\varepsilon^6 + \ldots\big]\,. \tag{3.28}$$

This perturbative result becomes important in the next Section. Exact numerical expressions for $\zeta^{\max}(k)$ are calculated from Eq. (3.27) via shooting [10, 71]. Performing a Legendre transform we find the rate functions $I(s)$. The left panel of Fig. 3.4 shows the rate function $I(s)$ for the white-noise model for $\varepsilon = 0.5$, 1.5 and 10 in black, blue and red, respectively. The right panel shows $I(s)$ in the persistent-flow models for $\kappa = 0.5$ (green), 1.5 (lime) and 10 (olive). Note that the location of the minimum of $I(s)$ is given by the Lyapunov exponent. Because the Lyapunov exponents change sign at finite inertia parameter, so do the locations of the minima of the rate functions. In both models, we observe that $I(s)$ becomes broader as the inertia parameter increases. This suggests that even if the (only) Lyapunov exponent is positive, particle trajectories may approach each other for a long time, allowing for spatial clustering even at positive Lyapunov exponent [71, 72].

3.4 Correlation dimension

The correlation dimension is given by the non-trivial zero of the scaled cumulant generating function $G_s(k)$ discussed in the previous Section [12, 18, 54, 73, 74]:

$$G_s(-D_2) = 0\,, \tag{3.29}$$

A derivation of this formula based on Ref. [74] is given in Appendix A. We now use (3.29) to calculate D_2 for the two models, starting with the white-noise

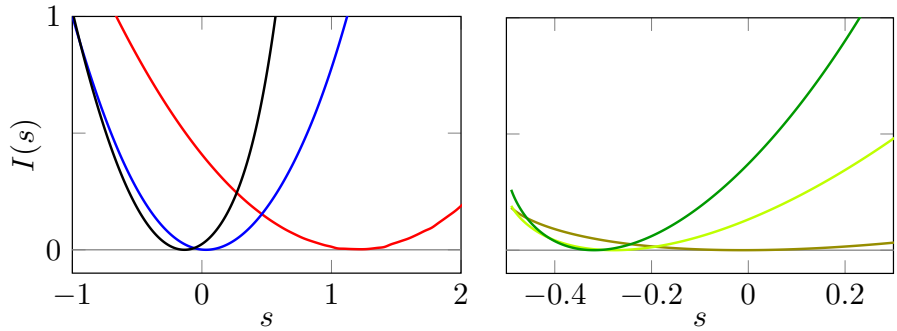

Figure 3.4: *Left:* Rate function $I(s)$ in the white-noise model for $\varepsilon = 0.5$, 1.5 and 10, black, blue and red, respectively. *Right:* Rate function $I(s)$ for persistent-flow model for $\kappa = 0.5$, 15 and 10, green, lime and olive, respectively.

model. Note that for the latter, the tilted-generator approach in combination with Eq. (3.29) is equivalent to a method of determining D_2 based on a separation ansatz for the Fokker-Planck equation, that was employed in [10, 54, 75] and paper B. Consider first the perturbative result for D_2 obtained from the perturbation expansion of $G_s(k)$ given in Eq. (3.28). The infinite series expression (3.28) is multiplied by $k(k-1)$. This means that $k^* = 1$ is a non-trivial root of $G_s(k)$ to all orders in perturbation theory. Hence, we find that the perturbation expansion of D_2 truncates after the first term [10, 54, 75]:

$$D_2 \sim -1\,. \tag{3.30}$$

How a negative correlation dimension in one dimension can be interpreted is discussed in paper B. Using the exact result for $G_s(k)$ calculated from numerically solving Eq. (3.27) we observe that Eq. (3.30) is a very poor approximation of D_2 at finite ε. The left panel in Fig. 3.5 shows D_2 obtained from Eq. (3.29) for the white-noise model as the red curve. In paper B we improved the asymptotic expansion (3.30) by an exponentially small correction

$$D_2 \sim -1 + \frac{\mathrm{e}^{-1/(6\varepsilon^2)}}{\pi}\,, \tag{3.31}$$

which is shown by the black dashed line in the left panel of Fig. 3.5. Details on the calculation are given in paper B. For larger ε, the correlation dimension increases and becomes positive for $\varepsilon > \varepsilon_c$. The same is true for the correlation

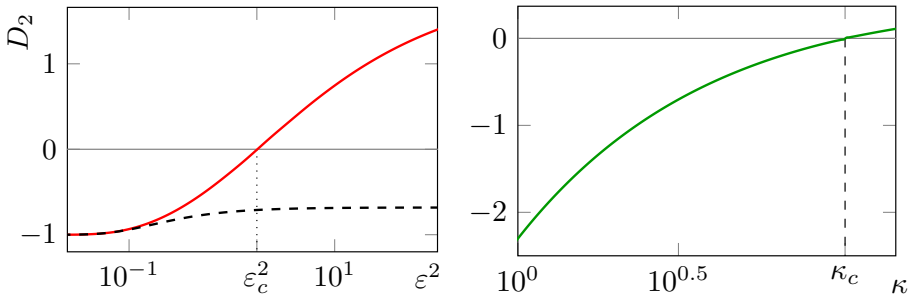

Figure 3.5: *Left:* Correlation dimension in the white-noise model shown in red, asymptotic expression (3.31) (black dashed line). *Right:* Correlation dimension for the persistent-flow model (green line).

dimension of the persistent-flow model which is given in the right panel of Fig. 3.5. The correlation dimension starts out at large negative values for small κ and becomes positive for $\kappa > \kappa_c \approx 10.4$.

3.4.1 Rate of caustic formation

We now briefly discuss explicit results for the activated form (2.25) of the rate of caustic formation at small inertial parameter. In the white-noise model, J can be obtained analytically and is given by the integral expression (3.22). For small ε the integral can be evaluated using a saddle point approximation, and one obtains [1]

$$J \sim \frac{\mathrm{e}^{-1/(6\varepsilon^2)}}{2\pi}. \tag{3.32}$$

Hence the activation function f defined in Eq. (2.25) is quadratic in Ku and linear in St, $f(\mathrm{Ku},\mathrm{St}) = 18\mathrm{Ku}^2\mathrm{St}$. In the persistent-flow model, we obtain the asymptotic form of J for small κ by analysing the tails in the distribution function $P(z(t)=z)$:

$$J \sim \frac{4\sqrt{2}}{\pi}\kappa^2 \mathrm{e}^{-\frac{1}{64\kappa^2}}, \tag{3.33}$$

which means that $f(\mathrm{Ku},\mathrm{St}) = 192\mathrm{Ku}^2\mathrm{St}^2$. For the telegraph model recall that there exists a regime in the (Ku, St) plane, where the rate of caustic formation is exactly zero, see right panel in Fig. 3.3. Around the regime border, a saddle point expansion similar to that for the white-noise model can be applied.

We find for the limit combined limit $\mathrm{St} \to \infty$ and $\mathrm{Ku} \to 0$ so that $\kappa = \sqrt{3}\mathrm{Ku}\,\mathrm{St}$ stays finite, the expression

$$J \sim \frac{1}{2\pi} \exp\left\{-2\mathrm{St}\left[\chi^- \operatorname{atan}(\chi^-) - \chi^+ \operatorname{atanh}(\chi^+)\right]\right\} \tag{3.34}$$

with $\chi^\pm = 1/\sqrt{4\kappa \pm 1}$ for $\kappa > 1/4$ and $J = 0$ otherwise. Note that the factor St can alternatively be written as $\mathrm{St} = \kappa/(\mathrm{Ku}\sqrt{3})$, which means that the expression is non-analytic in both $1/\mathrm{St}$ and Ku in the given limit. The activation function f has a non-polynomial form for the telegraph model.

3.5 Conclusions

We conclude that in one-dimensional statistical models the observables that characterise spatial clustering can be computed analytically or numerically with high accuracy. These one-dimensional results are very useful because the statistical models are similar in higher dimensions [1]. The different one-dimensional models share common features such as power-law tails in the z-distribution that scale with the respective rate of caustic formation and a path-coalescence transition [16, 48] as a function of their respective inertia parameter(s). Outside the path-coalescence phase, the one-dimensional models show clustering even though the spatial Lyapunov exponents is positive [72]. This is explained by the broad shape of the rate function for the FTLE [71].

Part II
Current and future work

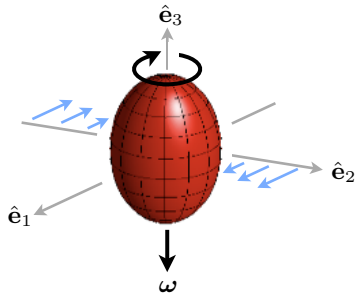

Figure 4.1: Spheroid in a shear flow in the log-rolling position. Taken from paper A.

4 Summary of research papers

In this Section we summarise the results of the three research papers A-C appended to this Licentiate thesis. In particular we explain how they are connected to the introductory text given in the previous Chapters.

4.1 Research paper A

In this paper, we calculated the angular velocity $\omega = \|\boldsymbol{\omega}\|$ of a small spheroidal particle in a simple shear flow in log-rolling position. In this position, the symmetry axis of the spheroid is oriented perpendicular to the shear plane, see Fig. 4.1, hence rendering the fluid dynamical problem steady. The characteristic Reynolds number defined in Section 1.3.1 is given by the shear Reynolds number

$$\mathrm{Re}_s = \frac{a^2 s}{\nu}, \tag{4.1}$$

where a is major semiaxis length of the particle, s is the shear rate and ν is the kinematic viscosity of the fluid. When Re_s is small, the angular velocity can be expanded in a perturbation series. As noted in Section 1.4.1 the convective term $(\boldsymbol{w}\cdot\nabla)\boldsymbol{w}$ constitutes a singular perturbation to the Stokes equation (1.14). Hence, regular perturbation theory breaks down far away from the particle. We used a matched asymptotic expansion of the flow field $\boldsymbol{w}$, see

Section 1.4.1, to obtain ω to order $\mathrm{Re}_\mathrm{s}^{3/2}$:

$$\omega \sim -\frac{s}{2} + 0.0540\frac{3sD}{10\pi}\mathrm{Re}_\mathrm{s}^{3/2}, \tag{4.2}$$

where D is a parameter that depends on the particle shape. We conducted direct numerical simulations of the problem and observed excellent agreement. In the special case of a sphere, where $D = 10\pi/3$, the result differs from that obtained in Ref. [76] by a factor of roughly three. The numerical simulations, however, support our results. Furthermore, in a recent study [77] the authors considered the case of general spheroid orientation (including log-rolling) and obtained Eq. (4.2) as a special case.

4.2 Research paper B

In paper B we studied the distribution of separations and relative velocities in polydisperse turbulent suspensions of heavy particles, using the statistical models discussed in Section 1.5 and Chapter 3. Systems of particles of different Stokes numbers are common in Nature which is why it is important to understand their dynamics. We studied these systems using the statistical model for of particles of *two* different Stokes numbers, St_1 and St_2. The first part of the work involved a numerical study of the two dimensional statistical model with finite Ku and St which we discussed in Section 1.3.3. For bidisperse systems, the different particle species obey two different sets of equations of motion (1.22), with St_1 and St_2, respectively. We observed that the distribution $\varrho(v_r, r)$ of relative velocities v_r between different Stokes-number particles develops a plateau at small separations r that cuts off the power-law distribution. The plateau is characterised by a cutoff scale v_c. A similar behaviour had been found for the spatial distribution in Refs. [13, 14] with the corresponding spatial cutoff scale r_c. Using a variant of the one-dimensional white-noise model discussed in Section 3.2.1, we were able to show that in one dimension, the scales v_c and r_c depend linearly upon the dimensionless quantity

$$\theta = \frac{|\mathrm{St}_1 - \mathrm{St}_2|}{\mathrm{St}_1 + \mathrm{St}_2}. \tag{4.3}$$

Interestingly, this linear dependence holds true even for the two-dimensional statistical model. The left panel in Fig. 4.2 shows how the plateau in $\varrho(v_r, r)$

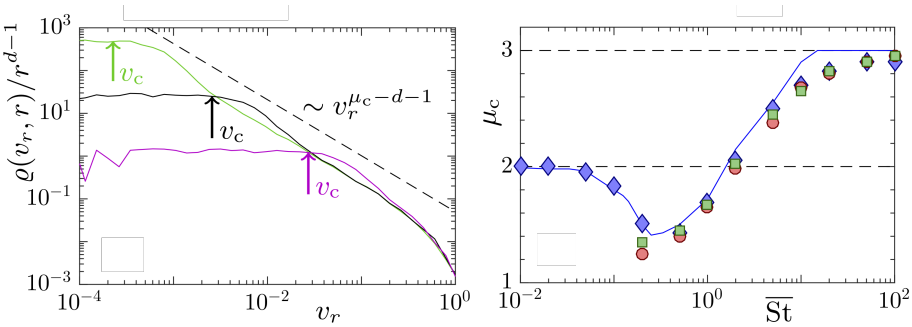

Figure 4.2: Statistical model simulations for $d = 2$, $\mathrm{Ku} = 1$ *Left:* $\varrho(v_r, r)/r^{d-1}$ evaluated for small r, $\overline{\mathrm{St}} = 1$ and $\theta = 10^{-3}$, 10^{-2} and 10^{-1} as the green, black and magenta lines, respectively. The crossover scales v_c are shown as arrows. *Right:* Power-law exponent μ_c as a function of $\overline{\mathrm{St}}$ for small θ. Exponent for the power-law tails in v_r for fixed small r with $\theta = 10^{-3}$ (green boxes) and $\theta = 10^{-2}$ (red circles). Exponent for power-law tails in r for fixed small v_r with $\theta = 10^{-2}$ (blue diamonds). Numerical data for μ_c (solid blue line). Figures taken from paper B.

at small r develops for $\theta = 10^{-3}$, 10^{-2} and 10^{-1} as the green, black and magenta lines, respectively. Further, we found that the spatial correlation dimension μ_c[1] of the monodisperse particle system discussed in Section 2.2.1, determines the shape of the tails in the bidisperse distribution $\varrho(v_r, r)$ when replacing the Stokes number by the mean Stokes number defined as

$$\overline{\mathrm{St}} = \frac{\mathrm{St}_1 \mathrm{St}_2}{\mathrm{St}_1 + \mathrm{St}_2}. \tag{4.4}$$

This holds both for the one-dimensional white-noise model and the two-dimensional statistical model. The right panel in Fig. 4.2 shows μ_c in the two-dimensional monodisperse model as a function of $\overline{\mathrm{St}}$ as the blue line. The symbols show the corresponding exponent in the tails of the bidisperse system. The tails for large r and small v_r, blue diamonds ($\theta = 10^{-3}$), and for large v_r and small r, green boxes and red circles ($\theta = 10^{-3}$ and 10^{-2}, respectively) have the same exponent just as in the monodisperse case [9].

[1]Note that here, the difference between the *spatial* correlation dimension μ_c and the *phase-space* correlation dimension D_2 is relevant. They are related by $\mu_c = \min[D_2, d]$, see Refs. [10, 53, 73].

We further found that finite θ regularises the path-coalescence transition, discussed in Secs. 2.1.4 and 3.3.2, in the one-dimensional bidisperse white-noise model. In the path-coalescence regime at small θ, the distribution of separations and relative velocities obtains power-law tails with negative correlation dimension $\mu_c < 0$. For small inertial parameter $\overline{\varepsilon} = 3\mathrm{Ku}^2\overline{\mathrm{St}}$ we were able to show that μ_c behaves asymptotically as

$$\mu_c \sim -1 + \frac{\mathrm{e}^{-1/(6\overline{\varepsilon}^2)}}{\pi}, \tag{4.5}$$

for $\overline{\varepsilon} \ll 1$. This can be written as $\mu_c \sim -1 + 2J$, where J is the rate of caustic formation in the model. This finding allows to interpret in physical terms earlier findings of negative correlation dimensions in the path-coalescence regime [9, 10, 75].

4.3 Research paper C

In this paper, we considered a one-dimensional, discrete-time model for inertial particles in fluid turbulence, the so-called correlated random walk model [72, 78]. In this model, the random displacements of an ensemble of walkers x_n are generated by a Gaussian random function $f_n(x) = u(x, t_n)$. This random function is identical to the one-dimensional random velocity field in Section 3.2, but uncorrelated in (discrete) time:

$$\langle f_n(x) f_m(y) \rangle = \alpha^2 \delta_{nm} \exp\left[-\frac{(x-y)^2}{2} \right], \tag{4.6}$$

where α is the dimensionless inertial parameter of the model. Due to the spatial correlations of the field $f_n(x)$, nearby walkers are correlated. The model shows similar behaviour as the one-dimensional continuous time white-noise model. Thus it exhibits a path-coalescence regime with associated negative correlation dimension. For small α one finds similarly to Eq. (4.5)

$$D_2 \sim -1 + 4 J_{\mathrm{CR}}, \tag{4.7}$$

where J_{CR} is the rate of trajectory crossings, which corresponds to the rate of caustic formation in continuous time. We identified a particularly simple kind of trajectory crossing in the model, which we called 'linear crossings'. Linear crossings are predominant at small separations and do not change the relative order of nearby walkers. Using an argument based on these crossings, we were able to use the scaling relation for D_q given in Eq. (2.17) to express D_q in terms of D_2:

$$D_q = \frac{D_2}{q-1}, \tag{4.8}$$

for $q > 2$. We confirmed this relation between the D_q numerically.

5 Conclusions and Outlook

In this Licentiate thesis, we discussed statistical models of heavy particles in turbulence. After motivating statistical models in Chapter 1 we focussed on their one-dimensional versions in Chapter 3 and paper C. In Chapter 4 and paper B, we showed that one-dimensional models are useful in explaining the results of statistical models in higher dimensions. Thus the distribution of separations and relative velocities between the heavy particles could be explained qualitatively using a one-dimensional white-noise model. The mathematical structure of the observables, the correlation dimension D_2, the finite-time Lyapunov exponents $\lambda(t)$ and the rate of caustic formation J, are richer than one might naively expect from the apparent simplicity of the one-dimensional models. On the basis of our results, we speculated in papers B and C that the correlation dimension must be represented by a 'trans-series' [79] of the form

$$D_2 \sim \sum_{k,l,m} a_{klm} \varepsilon^k \mathrm{e}^{-l\,s(\varepsilon)} \log^m[\varepsilon]\,, \tag{5.1}$$

in order to explain its characteristic dependence on the inertial parameter ε (α in paper C).

In the future, we want to study how this structure arises in two and three dimensional systems. The correlation dimension and the Lyapunov exponents in these higher-dimensional models have characteristic minima which are not explained by perturbation theory [16, 53, 54]. It would be interesting to understand if the locations of these minima can be calculated using trans-series expansions. In order to tackle this question mathematically, we need to find out if and how matched asymptotic expansions, that take into account rare caustic events, can be used in higher dimensions. Explaining these characteristic minima would be a great success, since it is observed also in simulations [49, 80].

A related but different problem concerns the Lyapunov exponent in the one-dimensional white-noise model. The perturbation expansion for this quantity is asymptotic [37] but can be resummed using Padé-Borél resummation [81]. The result agrees very well with the known analytic formula [1]. The Padé-Borél technique fails, however, for the Lyapunov exponent in the white-noise limits in two and three dimensions. The weak-inertia expansion

for the one-dimensional telegraph model is very similar to that of the white-noise limit. It is, however, more general and contains the weak-inertia limit of the white-noise model as a special case. Our plan is therefore to develop a perturbation theory for the weak-inertia limit of the telegraph model, to resum the corresponding series using Padé-Borél resummation, and compare the result to the exact expression, which is known in form of an integral [17]. This could explain why the perturbation theory for the Lyapunov exponent does *not* fail in the one-dimensional white-noise model. An analysis of this kind is relatively simple and could give important insights into the more ambitious question discussed in the previous paragraph.

Another future project concerns the realistic modelling of the statistics of velocity gradients in the one-dimensional persistent-flow model. As discussed in Section 3.2.3, this analysis must refer to non-local effects of preferential sampling of particles. Thus the particles spend most of their time at stable zeros of the flow $u(x,t)$. These zeros vanish at a certain rate, so that the particles travel possibly long distances before ending up at the next stable zero of $u(x,t)$. In the process, they sample positive velocity gradients which affects the velocity gradient statistics experienced by the particles measurably. We plan to use the properties of Gaussian random functions to find these gradient statistics.

Finally, it could be of interest to study the distribution of time intervals between caustics t_c, mentioned in Section 2.2.3. In the weak-inertia limit, this time is known to be exponentially distributed with mean $1/J$ [63]. At finite inertia, on the other hand, the distribution is different. It could be of interest to compare the probability distribution of t_c from the one-dimensional models with that in higher dimensional statistical models, and turbulence simulations. Caustics are considered essentially one-dimensional phenomena [18, 61]. Comparing the time distributions in different dimensions would put this statement to the test. We plan to approach this question using both theory and simulations. In the white-noise model the distribution of t_c can be calculated by interpreting t_c as the first-passage time from $z(0)=\infty$ to $z(t_c)=-\infty$ and solving a Backward-Kolmogorov equation [59, 60]. In the persistent-flow model the distribution is easily obtained analytically [61].

Bibliography

[1] GUSTAVSSON, K & MEHLIG, B 2016 Statistical models for spatial patterns of heavy particles in turbulence. *Advances in Physics* **65** (1), 1–57.

[2] PUMIR, A & WILKINSON, M 2016 Collisional aggregation due to turbulence. *Annual Review of Condensed Matter Physics* **7**, 141–170.

[3] SHAW, R. A 2003 Particle-turbulence interactions in atmospheric clouds. *Annu. Rev. Fluid Mech.* **35** (1), 183–227.

[4] BODENSCHATZ, E, MALINOWSKI, S. P, SHAW, R. A & STRATMANN, F 2010 Can we understand clouds without turbulence? *Science* **327** (5968), 970–971.

[5] DEVENISH, B. J, BARTELLO, P, BRENGUIER, J. L, COLLINS, L. R, GRABOWSKI, W. W, IJZERMANS, R. H, MALINOWSKI, S. P, REEKS, M. W, VASSILICOS, J. C, WANG, L. P & WARHAFT, Z 2012 Droplet growth in warm turbulent clouds. *Quarterly Journal of the Royal Meteorological Society* **138** (667), 1401–1429.

[6] FALKOVICH, G, FOUXON, A & STEPANOV, G 2002 Acceleration of rain initiation by cloud turbulence. *Nature* **419**, 151–154.

[7] WILKINSON, M & MEHLIG, B 2005 Caustics in turbulent aerosols. *Europhysics Letters* **71** (2), 186–192.

[8] WILKINSON, M, MEHLIG, B & BEZUGLYY, V 2006 Caustic activation of rain showers. *Physical Review Letters* **97** (4), 048501.

[9] GUSTAVSSON, K & MEHLIG, B 2011 Distribution of relative velocities in turbulent aerosols. *Physical Review E - Statistical, Nonlinear, and Soft Matter Physics* **84** (4), 045304.

[10] GUSTAVSSON, K & MEHLIG, B 2014 Relative velocities of inertial particles in turbulent aerosols. *Journal of Turbulence* **15** (1), 34–69.

[11] BEC, J 2003 Fractal clustering of inertial particles in random flows. *Physics of Fluids* **15** (11), 81–84.

[12] BEC, J, GAWEDZKI, K & HORVAI, P 2004 Multifractal clustering in compressible flows. *Physical Review Letters* **92** (22), 224501.

[13] BEC, J, CELANI, A, CENCINI, M & MUSACCHIO, S 2005 Clustering and collisions of heavy particles in random smooth flows. *Physics of Fluids (1994-present)* **17** (7), 073301.

[14] CHUN, J, KOCH, D. L, RANI, S. L, AHLUWALIA, A & COLLINS, L. R 2005 Clustering of aerosol particles in isotropic turbulence. *Journal of Fluid Mechanics* **536**, 219–251.

[15] FALKOVICH, G & PUMIR, A 2007 Sling Effect in Collisions of Water Droplets in Turbulent Clouds. *J. Atmos. Sci.* **64**, 4497–4505.

[16] WILKINSON, M & MEHLIG, B 2003 Path coalescence transition and its applications. *Physical Review E* **68** (4), 040101.

[17] FALKOVICH, G, MUSACCHIO, S, PITERBARG, L & VUCELJA, M 2007 Inertial particles driven by a telegraph noise. *Physical Review E* **76** (2), 026313.

[18] BEC, J, CENCINI, M, HILLERBRAND, R & TURITSYN, K 2008 Stochastic suspensions of heavy particles. *Physica D: Nonlinear Phenomena* **237**.

[19] HAPPEL, J & BRENNER, H 1983 *Low Reynolds Number Hydrodynamics*. Kluwer Academic Publishers Group.

[20] KIM, S & KARRILA, S. J 1991 *Microhydrodynamics: principles and selected applications*. Boston: Butterworth-Heinemann.

[21] NAVIER, C. L. M. H 1823 Memoire sur les lois du mouvement des fluides. *Memoires de l'Academie Royale des Sciences de l'Instit de France* **6**, 389–440.

[22] POPE, S. B 2000 *Turbulent flows*. Cambridge, UK: Cambridge University press.

[23] FRISCH, U 1997 *Turbulence*. Cambridge, UK: Cambridge University Press.

[24] YAVUZ, M. A, KUNNEN, R. P, VAN HEIJST, G. J & CLERCX, H. J 2018 Extreme Small-Scale Clustering of Droplets in Turbulence Driven by Hydrodynamic Interactions. *Physical Review Letters* **120** (24), 244504.

[25] ELGHOBASHI, S 1994 On predicting particle-laden turbulent flows. *Applied Scientific Research* **52** (4), 309–329.

[26] FALKOVICH, G, GAWEDZKI, K & VERGASSOLA, M 2001 Particles and fields in fluid turbulence. *Reviews of Modern Physics* **73** (4), 913–975.

[27] KOLMOGOROV, A. N 1941 The local structure of turbulence in incompressible viscous fluid for very large Reynolds numbers. *Doklady Akademii Nauk Sssr* **30** (4), 299–303.

[28] KOLMOGOROV, A. N 1941 Dissipation of energy in locally isotropic turbulence. *Proceedings of the USSR Academy of Sciences (Russian)* **32**, 16–18.

[29] RICHARDSON, L. F 2007 *Weather prediction by numerical process, second edition*. Cambridge University Press.

[30] SAW, E. W, SHAW, R. A, AYYALASOMAYAJULA, S, CHUANG, P. Y & GYLFASON, Á 2008 Inertial clustering of particles in high-reynolds-number turbulence. *Physical Review Letters* **100** (21), 214501.

[31] CVITANOVIC, P, ARTUSO, R, MAINIERI, R, TANNER, G, VATTAY, G, WHELAN, N & WIRZBA, A 2005 Chaos: classical and quantum. *ChaosBook. org (Niels Bohr Institute, Copenhagen 2005)* **69**.

[32] SHE, Z.-S, JACKSON, E & ORSZAG, S. A 1990 Intermittent vortex structures in homogeneous isotropic turbulence. *Nature* **344** (6263).

[33] GUSTAVSSON, K 2009 Advective collisions in random flows. Licentiate thesis, University of Gothenburg.

[34] CANDELIER, F, EINARSSON, J & MEHLIG, B 2016 Angular dynamics of a small particle in turbulence. *Physical Review Letters* **117** (20), 204501.

[35] VEYSEY, J & GOLDENFELD, N 2007 Simple viscous flows: From boundary layers to the renormalization group. *Reviews of Modern Physics* **79** (3), 883–927.

[36] HINCH, E. J 1991 *Perturbation Methods*. Cambridge: Cambridge University Press.

[37] BENDER, C. M & ORSZAG, S. A 1978 *Advanced Mathematical Methods for Scientists and Engineers*. New York, USA: McGraw-Hill.

[38] MAXEY, M. R & CORRSIN, S 1986 Gravitational settling of aerosol particles in randomly oriented cellular flow fields. *J. Atm. Sci* **43**, 1112–1134.

[39] MAXEY, M. R 1987 The gravitational settling of aerosol particles in homogeneous turbulence and random flow fields. *Journal of Fluid Mechanics* **174**, 441–465.

[40] GUSTAVSSON, K, VAJEDI, S & MEHLIG, B 2014 Clustering of particles falling in a turbulent flow. *Physical Review Letters* **112** (21), 214501.

[41] BEC, J, HOMANN, H & RAY, S. S 2014 Gravity-driven enhancement of heavy particle clustering in turbulent flow. *Physical Review Letters* **112** (18), 184501.

[42] GUSTAVSSON, K, MENEGUZ, E, REEKS, M & MEHLIG, B 2012 Inertial-particle dynamics in turbulent flows: Caustics, concentration fluctuations and random uncorrelated motion. *New Journal of Physics* **14** (11), 115017.

[43] GUSTAVSSON, K & MEHLIG, B 2011 Ergodic and non-ergodic clustering of inertial particles. *EPL* **96** (6), 60012.

[44] WANG, L & MAXEY, M. R 1993 Settling velocity and concentration distribution of heavy particles in homogeneous isotropic turbulence. *J. Fluid Mech.* **256**, 27–68.

[45] BEC, J, BIFERALE, L, BOFFETTA, G, CENCINI, M, MUSACCHIO, S & TOSCHI, F 2006 Lyapunov exponents of heavy particles in turbulence. *Physics of Fluids* **18** (9), 091702.

[46] BEC, J, BIFERALE, L, CENCINI, M, LANOTTE, A, MUSACCHIO, S & TOSCHI, F 2007 Heavy particle concentration in turbulence at dissipative and inertial scales. *Physical Review Letters* **98** (8), 084502.

[47] WILKINSON, M, MEHLIG, B, ÖSTLUND, S & DUNCAN, K. P 2007 Unmixing in random flows. *Physics of Fluids* **19** (11), 113303.

[48] DEUTSCH, J. M 1985 Aggregation-disorder transition induced by fluctuating random forces. *Journal of Physics A: General Physics* **18** (9), 1449.

[49] BEC, J, BIFERALE, L, CENCINI, M, LANOTTE, A. S & TOSCHI, F 2011 Spatial and velocity statistics of inertial particles in turbulent flows. *Journal of Physics: Conference Series* **333** (1), 012003.

[50] BEC, J 2005 Multifractal concentrations of inertial particles in smooth random flows. *J. Fluid Mech.* **528**, 255–277.

[51] OTT, E 2002 *Chaos in dynamical systems, 2nd edition*. Cambridge, UK: Cambridge Univeristy Press.

[52] HARTE, D 2001 *Multifractals: theory and applications*. Chapman and Hall/CRC.

[53] WILKINSON, M, MEHLIG, B & GUSTAVSSON, K 2010 Correlation dimension of inertial particles in random flows. *EPL* **89** (5), 50002.

[54] GUSTAVSSON, K, MEHLIG, B & WILKINSON, M 2015 Analysis of the correlation dimension of inertial particles. *Phys. Fluids* **27** (7), 073305.

[55] GRASSBERGER, P & PROCACCIA, I 1983 Measuring the strangeness of Attractors. *Physica D: Nonlinear Phenomena* **9** (1-2), 189–208.

[56] SCHOMERUS, H & TITOV, M 2002 Statistics of finite-time Lyapunov exponents in a random time-dependent potential. *Physical Review E* **66** (6), 066207.

[57] TOUCHETTE, H 2009 The large deviation approach to statistical mechanics. *Physics Reports* **478** (1), 1–69.

[58] GRIMMETT, G & STIRZAKER, D 2001 *Probability and Random Processes*. Oxford University Press.

[59] VAN KAMPEN, N 2007 Stochastic Processes in Physics and Chemistry. In *Stochastic Processes in Physics and Chemistry*. Elsevier.

[60] GARDINER, C. W 2009 *Handbook of Stochastic Methods: For the Natural and Social Sciences*. Springer.

[61] DEREVYANKO, S. A, FALKOVICH, G, TURITSYN, K & TURITSYN, S 2016 Lagrangian and Eulerian descriptions of inertial particles in random flows. *Journal of Turbulence* **8** (No. 16).

[62] CHETRITE, R, FALKOVICH, G & GAWEDZKI, K 2008 Fluctuation relations in simple examples of non-equilibrium steady states. *Journal of Statistical Mechanics: Theory and Experiment* **2008** (08), P08005.

[63] MEHLIG, B & WILKINSON, M 2004 Coagulation by random velocity fields as a Kramers problem. *Physical Review Letters* **92** (25), 250602.

[64] RICE, S. O 1944 Mathematical analysis of random noise. *Bell System Technical Journal* **23** (3), 282–332.

[65] KAC, M 1948 On the average number of real roots of a random algebraic equation. *Proceedings of the London Mathematical Society* **2** (1), 390–408.

[66] GUSTAVSSON, K & MEHLIG, B 2013 Lyapunov Exponents for Particles Advected in Compressible Random Velocity Fields at Small and Large Kubo Numbers. *Journal of Statistical Physics* **153** (5), 813–827.

[67] MEHLIG, B, WILKINSON, M, BEZUGLYY, V, GUSTAVSSON, K & NAKAMURA, K 2009 Multiple regimes of diffusion. *Phys. Rev. E* **80**, 011139.

[68] SHAPIRO, V. E & LOGINOV, V. M 1978 Formulae of differentiation and their use for solving stochastic equations. *Physica A* **91**, 563–574.

[69] GÄRTNER, J 1977 On Large Deviations from the Invariant Measure. *Theory of Probability & Its Applications* **22** (1), 24–39.

[70] ELLIS, R. S 2007 *Entropy, large deviations, and statistical mechanics*. Springer.

[71] HUBER, G, PRADAS, M, PUMIR, A & WILKINSON, M 2018 Persistent stability of a chaotic system. *Physica A: Statistical Mechanics and its Applications* **492**, 517–523.

[72] WILKINSON, M, MEHLIG, B, GUSTAVSSON, K & WERNER, E 2012 Clustering of exponentially separating trajectories. *The European Physical Journal B* **85** (1), 18.

[73] BEC, J, CENCINI, M & HILLERBRAND, R 2007 Heavy particles in incompressible flows: The large Stokes number asymptotics. *Physica D: Nonlinear Phenomena* **226** (1), 11–22.

[74] PIKOVSKY, A. S 1992 Statistics of trajectory separation in noisy dynamical systems. *Physics Letters A* **165** (1), 33–36.

[75] WILKINSON, M, GUICHARDAZ, R, PRADAS, M & PUMIR, A 2015 Power-law distributions in noisy dynamical systems. *EPL* **111** (5), 50005.

[76] LIN, C.-J, PEERY, J. H & SCHOWALTER, W. R 1970 Simple shear flow round a rigid sphere: inertial effects and suspension rheology. *Journal of Fluid Mechanics* **44** (01), 1–17.

[77] MARATH, N. K & SUBRAMANIAN, G 2017 The effect of inertia on the time period of rotation of an anisotropic particle in simple shear flow. *Journal of Fluid Mechanics* **830**, 165–210.

[78] PRADAS, M, PUMIR, A, HUBER, G & WILKINSON, M 2017 Convergent chaos. *Journal of Physics A: Mathematical and Theoretical* **50** (27), 275101.

[79] DORIGONI, D 2014 An introduction to resurgence, trans-series and alien calculus. *arXiv preprint arXiv:1411.3585* .

[80] BHATNAGAR, A, GUSTAVSSON, K & MITRA, D 2018 Statistics of the relative velocity of particles in turbulent flows: Monodisperse particles. *Physical Review E* **97** (2), 23105.

[81] ELETSKY, V. L & POPOV, V. S 1978 On the Padé-Borel summation of perturbation series. *Physics Letters B* **77** (4-5), 411–414.

[82] MEIBOHM, J, CANDELIER, F, ROSÉN, T, EINARSSON, J, LUNDELL, F & MEHLIG, B 2016 Angular velocity of a spheroid log rolling in a simple shear at small Reynolds number. *Physical Review Fluids* **1** (8), 084203.

[83] MEIBOHM, J, PISTONE, L, GUSTAVSSON, K & MEHLIG, B 2017 Relative velocities in bidisperse turbulent suspensions. *Physical Review E* **96** (6), 061102.

[84] DUBEY, A, MEIBOHM, J, GUSTAVSSON, K & MEHLIG, B 2018 Fractal dimensions and trajectory crossings in correlated random walks. *arXiv preprint arXiv:1806.08207* .

PART III
APPENDIX

A Correlation dimension and FTLE

We now prove the relation (3.29). The proof goes along the same lines as that given in Ref. [74] for discrete noisy dynamical systems. Consider the equations of motion for the white-noise model (3.10):

$$\dot{j}(t) = z(t)j(t), \tag{A.1a}$$

$$\dot{z}(t) = \xi_t - z(t) - z(t)^2. \tag{A.1b}$$

Transforming $j(t)$ in Eq. (A.1a) into $y(t) = \log|j(t)|$, we obtain $\dot{y}(t) = z(t)$. If we now integrate both sides of this equation from 0 to $t_n = nT$ with $T \gg 1$ we obtain

$$X_n = \int_0^{t_n} z(t)\mathrm{d}t\,, \tag{A.2}$$

where $X_n = y(t_n) - y(0) = \log|j(t_n)|$. The random variables X_n obey the recurrence

$$X_{n+1} = X_n + T\lambda_n\,, \tag{A.3}$$

with $\lambda_n = T^{-1}\int_{t_n}^{t_{n+1}} z(t)\mathrm{d}t = \lambda(T)$. In the last step we noted that λ_n is equal to the spatial FTLE, $\lambda(T)$, of the system. Since $T \gg 1$, λ_n obeys a large deviation principle according to

$$P(\lambda_n = s) \approx \mathrm{e}^{-TI(s)}. \tag{A.4}$$

For long enough T, and sufficiently quickly decaying correlation function $c(|t-s|) = \langle z(t)z(s)\rangle - \langle z(t)\rangle\langle z(s)\rangle$, we can treat X_n and λ_n as independent random variables. Hence, Eq. (A.3) suggests that the probability density for X_{n+1}, $P(X_{n+1} = x)$, is given by the convolution

$$P(X_{n+1} = x) = \int_{-\infty}^{\infty} P(\lambda_n = s)P(X_n = x - Ts)\mathrm{d}s\,. \tag{A.5}$$

In the steady state, X_{n+1} and X_n are equal in distribution, which means that $P(X_{n+1}=x)=P(X_n=x)$. Substituting this condition into Eq. (A.5) we obtain an integral equation for $P(X_n=x)$ with solution $P(X_n=x)\sim \mathrm{e}^{\mu x}$, involving the constant μ. Because $X_n=\log|j(t_n)|$, the density of $j(t)$ is given by the power-law

$$P(j(t)=x)\sim x^{\mu-1}\,. \tag{A.6}$$

We compare this expression to the scaling relation (2.17) and recall that $j(t)$ has the same dynamics as the particle pair separation $|x_1(t)-x_2(t)|$. Using this we conclude that $\mu=D_2$. We now substitute the expression for $P(X_n=x)$ into Eq. (A.5) and use the large deviation form (A.4). We obtain

$$\int_{-\infty}^{\infty}\mathrm{e}^{-T(I(s)+D_2 s)}\mathrm{d}s\approx 1\,, \tag{A.7}$$

which we, in turn, evaluate using Laplace's method for $T\gg 1$ [37]. We arrive at the asymptotic relation $\exp[-TG_s(-D_2)]\approx 1$, where

$$G_s(k)=\inf_{s\in\mathbb{R}}(I(s)-ks)=\sup_{s\in\mathbb{R}}(ks-I(s))\,, \tag{A.8}$$

is the scaled cumulant generating function of the FTLE. Clearly this derivation suggests that

$$G_s(-D_2)=0\,, \tag{A.9}$$

which is what we wanted to show. Note that $\mu=0$ and, thus $P(X_n=x)=\text{const}$ is another, trivial solution of Eq. (A.5). This trivial solution is independent of the underlying dynamics, and comes solely from the normalisation of $P(\lambda_n=s)$ to unity. We conclude that the non-zero root of $G_s(k)$ is the physical one.

Part IV
Research papers

Paper A

https://doi.org/10.1103/PhysRevFluids.1.084203

Paper B

https://doi.org/10.1103/PhysRevE.96.061102

Paper C

https://arxiv.org/abs/1806.08207